Applying the density matrix expansion with coordinate-space chiral interactions

A. Dyhdalo,[1,*] S. K. Bogner,[2,†] and R. J. Furnstahl[1,‡]
[1]*Department of Physics, Ohio State University, Columbus, Ohio 43210, USA*
[2]*National Superconducting Cyclotron Laboratory and Department of Physics and Astronomy, Michigan State University, East Lansing, Michigan 48824, USA*

(Received 31 January 2017; revised manuscript received 1 March 2017; published 22 May 2017)

We apply the density matrix expansion (DME) at Hartree-Fock level with long-range chiral effective field theory interactions defined in coordinate space up to next-to-next-to-leading order. We consider chiral potentials both with and without explicit Δ isobars. The challenging algebra associated with applying the DME to three-nucleon forces is tamed using a new organization scheme, which will also facilitate generalizations. We include local regulators on the interactions to mitigate the effects of singular potentials on the DME couplings and simplify the optimization of generalized Skyrme-like functionals.

DOI: 10.1103/PhysRevC.95.054314

I. INTRODUCTION

Despite great progress in recent years in *ab initio* methods, solving the quantum many-body problem for the entire range of nuclei is currently only feasible with phenomenological energy density functionals (EDFs) [1]. These methods, which are often justified by theorems from density functional theory, have favorable computational scaling to large systems and can be used to compute observables such as binding energies, radii, electromagnetic transitions, β-decay rates, and fission cross sections across the nuclear chart [1,2]. Skyrme functionals [3,4] are a type of EDF utilizing *local* nuclear densities and their gradients, such as would result from zero-range interactions treated at the Hartree-Fock level. These functionals are usually supplemented with a pairing interaction to account for nuclear superfluidity [1,5–8]. The functional is specified by of order ten parameters, which are fitted to a subset of nuclear data. An extensive infrastructure for optimizing and applying Skyrme EDFs has been developed [9–13].

The best Skyrme parametrizations have had many phenomenological successes, but there are clear limitations. A systematic way to improve these functionals within the Skyrme framework has not been demonstrated and extrapolations to nuclei for which no data exist are often model dependent, which hinders uncertainty quantification. Sophisticated analyses have concluded that with the standard form, the accuracy of masses and other observables has reached a limit [14–17]. Yet improving the global performance of mass models is desirable to constrain nuclear reactions, e.g., for r-process nucleosynthesis [18,19]. In previous work, a program was initiated to address these issues by incorporating microscopic physics in Skyrme EDFs using an improved version of the density matrix expansion (DME) [20–23]. The idea is that existing functionals may have too simplistic density dependencies to account for long-range pion physics, but they can be incorporated with the DME while still taking advantage of the Skyrme infrastructure. Here we present a new implementation of the DME in coordinate space using pion-exchange interactions with local regulators.

We adopt the organization of pion-range physics given by chiral effective field theory, χEFT, including both nucleon-nucleon (NN) and three-nucleon ($3N$) forces [24,25]. χEFT provides a model-independent low-energy expansion of the long-range forces between nucleons; see Refs. [26–28] for reviews. The relevant degrees of freedom are asymptotic nucleon states and pions, with Δ isobars sometimes added to improve the convergence of the expansion [29,30]. The resulting chiral potentials have had many successes in recent calculations of nuclear phenomena [31–45]. By including these chiral potentials, we set the stage for connecting the physics of QCD to calculations of the full table of nuclides. In the present work, the physics of the chiral potentials is manifested in a generalized Skyrme EDF as density-dependent couplings multiplying bilinears and trilinears of the local densities. These chiral couplings are derived starting from Hartree-Fock in many-body perturbation theory (MBPT). The chiral physics will not be explicitly built into pairing terms as we expect the pairing channel to be well represented by contact interactions.

We are not yet ready to "replace phenomenological models of nuclear structure and reactions with a well-founded microscopic theory that delivers maximum predictive power with well-quantified uncertainties" [8, p. 2236] via the construction of a fully *ab initio* functional based on model-independent chiral interactions. Even working with renormalization group softened interactions [46], it is necessary to go to at least second order in MBPT for convergence in infinite matter [47]. Instead, we follow the semiphenomenological philosophy outlined in Refs. [20,21] and implemented in Refs. [22,23]. The idea is to add in the microscopic pion and Δ physics from the chiral potentials using MBPT *without* including the systematic short-range terms from free-space power counting;[1] instead afterwards a global refit of the Skyrme parameters is

*dyhdalo.2@osu.edu
†bogner@nscl.msu.edu
‡furnstahl.1@osu.edu

[1]Note that we also do not include the contribution from the intermediate-range N^{2}LO $3N$ interaction (see Sec. III).

performed. The chiral couplings are parameter-free in the sense that they are frozen while the Skyrme contacts are adjusted to data. Thus, this is an intermediate approach between *ab initio* and phenomenology that seeks to constrain the form and couplings of the functional via the underlying vacuum NN and $3N$ interactions [48,49]. This enables a comparison with conventional Skyrme EDFs to assess the role of explicit pion and Δ physics in nuclear structure.

When working with finite-range potentials, Fock energy terms in MBPT consist of one-body density matrices (OBDMs), which are inherently nonlocal objects, including correlations between spatially separated points. This nonlocality in the OBDM significantly complicates the iteration and computational cost of solving the Skyrme Hartree-Fock-Bogoliubov equations. The DME, first formulated by Negele and Vautherin in Refs. [50,51], provides a general way to map nonlocal functionals into local ones by converting OBDMs into local densities. In particular, the nonlocality in the OBDMs arising from the finite-range potentials is factorized into products of local densities multiplied by density-dependent couplings. The expansion is *not* a naive Taylor expansion about the OBDM diagonal but instead resums certain contributions such that it is an expansion about the homogeneous nuclear matter limit. The DME is not uniquely defined; in this paper we adopt the phase-space-averaging formulation of Ref. [20], which showed dramatic improvements in reproducing the vector parts of the OBDM over the original Negele-Vautherin prescription.

The algebraic complexity of applying the DME rapidly increases as one goes from NN to $3N$ forces, which necessitates a robust yet practical organization scheme. As part of a previous DME implementation using chiral forces, the spin-isospin traces over the N^{2}LO three-body diagrams were carried out in Ref. [52] using symbolic software, with an emphasis on analytic derivation of the couplings. The DME for the chiral potentials was implemented in momentum space and did not include ultraviolet regulators. The resulting functional was then used in preoptimization tests in Ref. [22]. While it showed indications of slight improvements in the reproduction of data, there were notable complications with stability and optimization. An alternative implementation of the DME with chiral potentials is given in Ref. [53].

We instead derive the couplings in coordinate space, using a new organization scheme, and numerically perform the final integrals. The resulting DME algebra is much simpler for the $3N$ potentials. Coordinate-space chiral potentials have been recently applied in quantum Monte Carlo calculations in Refs. [54–57], and allow the natural use of coordinate-space regulators. There are several reasons to take this approach:

(1) The DME is most naturally formulated as an expansion in coordinate space. Working with a coordinate space interaction simplifies the DME coupling calculations, as no Fourier integrals need to be done.
(2) The use of regulators has been shown to have a significant influence on many-body calculations even at the Hartree-Fock level [58,59]. Using regulators allows for the DME couplings to be less affected by the singular short-distance parts of the chiral potentials.
(3) Coordinate-space interactions allow for the natural implementation of local coordinate-space regulators. These regulators are thought to suppress more effectively the singular parts of the one-pion-exchange (OPE) tensor and two-pion-exchange (TPE) potentials and have smaller artifacts than alternative nonlocal, momentum-space regulators. Recent calculations imply that the convergence of the chiral expansion for certain NN cross sections is more systematic with such regulators [60].
(4) By including a regulator and varying the cutoff, we allow for an adiabatic turning on the finite-range physics. This enables a more controlled and stable implementation of the EDF optimization, as one can bootstrap the finite-range forces starting from the well-studied parameter space of conventional Skyrme functionals.

The plan of the paper is as follows. In Sec. II, we set up the framework starting from Hartree-Fock for two- and three-body forces. The NN and $3N$ coordinate-space chiral potentials used in this paper, along with the chosen regularization scheme, are described in Sec. III. The relevant quantities in our EDF, the form of the EDF, and the DME parametrization are enumerated in Sec. IV. In Secs. V and VI, we perform the DME for NN and $3N$ forces, respectively. Sample results for the NN and $3N$ DME-derived couplings are shown in Sec. VII and Sec. VIII has a summary and outlook for the next steps in this program. Detailed derivations, formulas, and MATHEMATICA notebooks are collected in the Supplemental Material [61].

II. HARTREE-FOCK FOR NN AND $3N$ FORCES

The Hartree-Fock energy for an antisymmetrized two-body potential is given by

$$V_{\rm HF}^{\rm NN} = \frac{1}{2}\sum_{ij}\langle ij|\mathcal{V}^{\rm NN}|ij\rangle\,, \tag{1}$$

with the sums over occupied orbitals and the antisymmetrized NN interaction and exchange operators defined as

$$\mathcal{V}^{\rm NN} \equiv V^{\rm NN}(1-P_{12}), \quad P_{12} \equiv P^{\sigma}P^{\tau}P^{r}, \tag{2}$$

where

$$P_{12}^{\sigma} = \tfrac{1}{2}(1+\boldsymbol{\sigma}_1\cdot\boldsymbol{\sigma}_2), \quad P_{12}^{\tau} = \tfrac{1}{2}(1+\boldsymbol{\tau}_1\cdot\boldsymbol{\tau}_2). \tag{3}$$

By inserting resolutions of the identity,

$$1 = \sum_{\sigma\tau}\int d\mathbf{r}\,|\mathbf{r}\sigma\tau\rangle\langle\mathbf{r}\sigma\tau|\,, \tag{4}$$

Eq. (1) can be rendered in coordinate space:

$$V_{\rm HF}^{\rm NN} = \frac{1}{2}\sum_{\sigma\tau}\int\prod_{i=1}^{4}d\mathbf{r}_i\;\langle\mathbf{r}_1\sigma_1\tau_1\;\mathbf{r}_2\sigma_2\tau_2|\mathcal{V}^{\rm NN}|\mathbf{r}_3\sigma_3\tau_3\;\mathbf{r}_4\sigma_4\tau_4\rangle \times\rho_1(\mathbf{r}_3\sigma_3\tau_3,\mathbf{r}_1\sigma_1\tau_1)\,\rho_2(\mathbf{r}_4\sigma_4\tau_4,\mathbf{r}_2\sigma_2\tau_2). \tag{5}$$

The ρ terms are the OBDMs that encapsulate all the information about the Hartree-Fock orbitals,

$$\rho(\mathbf{r}_3\sigma_3\tau_3,\mathbf{r}_1\sigma_1\tau_1) \equiv \sum_i \phi_i^*(\mathbf{r}_1\sigma_1\tau_1)\phi_i(\mathbf{r}_3\sigma_3\tau_3), \tag{6}$$

where the sum runs over the occupied orbitals in the system. The OBDM subscript 1 (2) in Eq. (5) defines the term to act on the first (second) part of the two-body product space. Extending the formalism to include pairing via Hartree-Fock-Bogoliubov, the orbital occupation in Eq. (6) becomes fractional [1]. Note again that we are only including chiral physics in the particle-hole channel as the pairing channel will be represented by contact interactions.

Switching to relative ($\mathbf{r}$) and center-of-mass ($\mathbf{R}$) coordinates and assuming translational invariance and locality of the potential, two of the coordinate space integrals can be done. Omitting the spin-isospin arguments in the OBDMs, Eq. (5) then becomes

$$\begin{aligned} V_{\rm HF}^{\rm NN} = \frac{1}{2}{\rm Tr}_1{\rm Tr}_2 \int d\mathbf{R}d\mathbf{r}\ \langle \mathbf{r}\sigma_1\tau_1\sigma_2\tau_2|V^{\rm NN}|\mathbf{r}\sigma_3\tau_3\sigma_4\tau_4\rangle \\ \times \left[\rho_1\left(\mathbf{R}+\frac{\mathbf{r}}{2}\right)\rho_2\left(\mathbf{R}-\frac{\mathbf{r}}{2}\right) - \rho_1\left(\mathbf{R}-\frac{\mathbf{r}}{2},\mathbf{R}+\frac{\mathbf{r}}{2}\right)\right. \\ \left.\times\, \rho_2\left(\mathbf{R}+\frac{\mathbf{r}}{2},\mathbf{R}-\frac{\mathbf{r}}{2}\right)P_{12}^{\sigma\tau}\right], \end{aligned} \tag{7}$$

where

$$\rho(\mathbf{x},\mathbf{x}) \equiv \rho(\mathbf{x}), \tag{8}$$

and the traces ${\rm Tr}_1$, ${\rm Tr}_2$ are over the spin-isospin parts of our product space. The first term in brackets is the direct (Hartree) term while the second is the exchange (Fock) term.

As the OBDMs for the Hartree term are diagonal, they are written as products of local densities multiplying a finite-range potential. Although it is possible to apply the DME to the Hartree term as well, in practice error propagation in the self-consistent iteration is reduced when applying the DME only to the Fock term [51,62]. Treating the Hartree term exactly also provides a better reproduction of the full Hartree-Fock energy and density fluctuations [23,51]. This exact treatment does not cause a significant increase in computational complexity when solving for self-consistency [23,51].

The Hartree-Fock energy for a three-body potential is given by

$$V_{\rm HF}^{\rm 3N} = \frac{1}{6}\sum_{ijk}\langle ijk|V^{\rm 3N}(1+P_{13}P_{12}+P_{23}P_{12})(1-P_{12})|ijk\rangle, \tag{9}$$

where again the sums are over occupied orbitals, and $V^{\rm 3N}$ refers to the full three-body force [see Eq. (22) below] with the various exchange operators accounting for three-body antisymmetry. Using the symmetry of $V^{\rm 3N}$ under subscript interchange, Eq. (9) can be rewritten using only one of the three-body potentials [48],

$$V_{\rm HF}^{\rm 3N} = \frac{1}{2}\sum_{ijk}\langle ijk|V_{23}(1-2P_{12}-P_{23}+2P_{23}P_{12})|ijk\rangle. \tag{10}$$

Therefore, there is one direct or Hartree term (H) and two exchange pieces. The sum of the single exchange (SE) and the double exchange (DE) terms give us our Fock (F) term,

$$V_{\rm H}^{\rm 3N} \equiv \frac{1}{2}\sum_{ijk}\langle ijk|V_{23}|ijk\rangle, \tag{11a}$$

$$V_{\rm SE,\,F}^{\rm 3N} \equiv \frac{1}{2}\sum_{ijk}\langle ijk|V_{23}(-2P_{12}-P_{23})|ijk\rangle, \tag{11b}$$

$$V_{\rm DE,\,F}^{\rm 3N} \equiv \sum_{ijk}\langle ijk|V_{23}P_{23}P_{12}|ijk\rangle, \tag{11c}$$

$$V_{\rm F}^{\rm 3N} \equiv V_{\rm SE,\,F}^{\rm 3N} + V_{\rm DE,\,F}^{\rm 3N}. \tag{11d}$$

Analogously to the NN sector, for the $3N$ sector we again insert completeness relations and work in coordinate space, encapsulating information about the Hartree-Fock orbitals in the OBDMs. The spin-isospin part of the exchange operator is kept with the interaction while the spatial part of the exchange operator acts on the arguments of the OBDMs. Enforcing the locality of our potential and suppressing the spin and isospin arguments in the OBDMs and potential, we find [52,63]

$$V_{\rm H}^{\rm 3N} = \frac{1}{2}{\rm Tr}_1{\rm Tr}_2{\rm Tr}_3 \int d\mathbf{r}_1 d\mathbf{r}_2 d\mathbf{r}_3\ \rho_1(\mathbf{r}_1)\rho_2(\mathbf{r}_2)\rho_3(\mathbf{r}_3)\ V_{23}(\mathbf{r}_{21},\mathbf{r}_{31}), \tag{12a}$$

$$\begin{aligned} V_{\rm SE,\,F}^{\rm 3N} = &-{\rm Tr}_1{\rm Tr}_2{\rm Tr}_3 \int d\mathbf{r}_1 d\mathbf{r}_2 d\mathbf{r}_3\ \rho_1(\mathbf{r}_2,\mathbf{r}_1)\rho_2(\mathbf{r}_1,\mathbf{r}_2)\rho_3(\mathbf{r}_3)\ V_{23}(\mathbf{r}_{21},\mathbf{r}_{31})\ P_{12}^{\sigma\tau} \\ &-\frac{1}{2}{\rm Tr}_1{\rm Tr}_2{\rm Tr}_3 \int d\mathbf{r}_1 d\mathbf{r}_2 d\mathbf{r}_3\ \rho_1(\mathbf{r}_1)\rho_2(\mathbf{r}_3,\mathbf{r}_2)\rho_3(\mathbf{r}_2,\mathbf{r}_3)\ V_{23}(\mathbf{r}_{21},\mathbf{r}_{31})\ P_{23}^{\sigma\tau}, \end{aligned} \tag{12b}$$

$$V_{\rm DE,\,F}^{\rm 3N} = {\rm Tr}_1{\rm Tr}_2{\rm Tr}_3 \int d\mathbf{r}_1 d\mathbf{r}_2 d\mathbf{r}_3\ \rho_1(\mathbf{r}_3,\mathbf{r}_1)\rho_2(\mathbf{r}_1,\mathbf{r}_2)\rho_3(\mathbf{r}_2,\mathbf{r}_3)\ V_{23}(\mathbf{r}_{21},\mathbf{r}_{31})\ P_{23}^{\sigma\tau}P_{12}^{\sigma\tau}, \tag{12c}$$

where the traces go over the spin and isospin of the three particles. For the purposes of performing the DME in the $3N$ system, the above equations must be converted into a more convenient form. We instead work with the variables

$$\mathbf{r}_1, \quad \mathbf{x}_2 = \mathbf{r}_{21}, \quad \mathbf{x}_3 = \mathbf{r}_{31}, \tag{13}$$

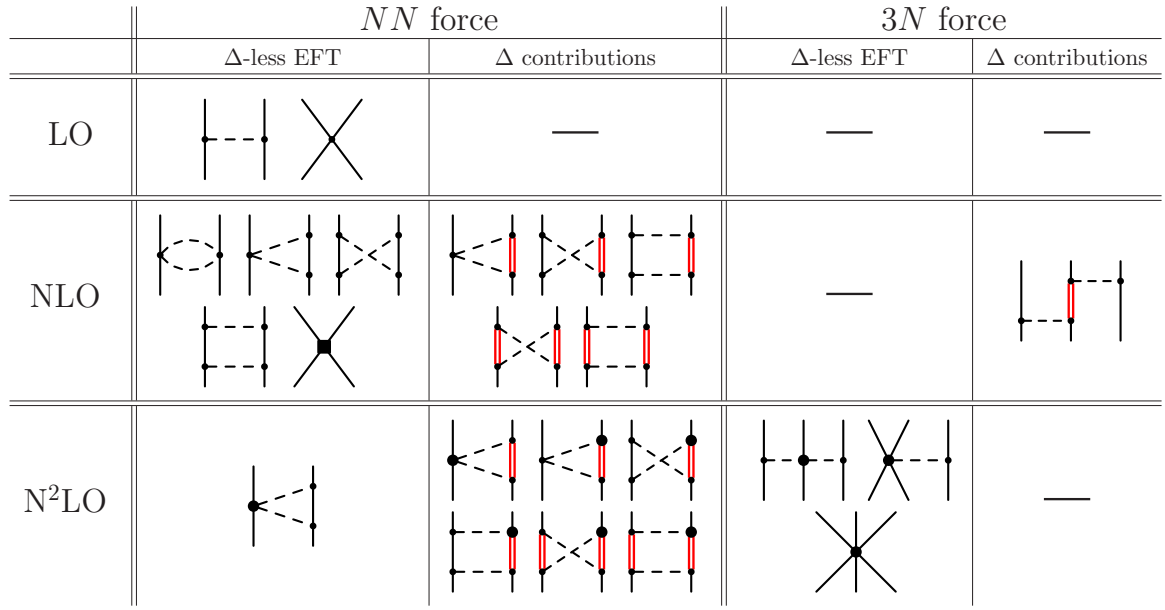

FIG. 1. Diagrams in the chiral expansion up to N^{2}LO for NN and $3N$ forces. Solid lines are nucleons, dashed lines are pions, and double solid lines (red) are Δ isobars. Small dots, filled circles, and squares denote vertices of chiral index 0, 1, and 2, respectively [27]. Only one representative example of each type of diagram has been shown. In the Δ-less theory, only the diagrams in the two corresponding columns contribute to the potential. In the theory with Δs, all the columns contribute.

where the Jacobian of the transformation is unity. Applying this transformation yields

$$V_{\rm H}^{\rm 3N} = \frac{1}{2}{\rm Tr}_1{\rm Tr}_2{\rm Tr}_3 \int d\mathbf{r}_1 d\mathbf{x}_2 d\mathbf{x}_3 \; \rho_1(\mathbf{r}_1)\rho_2(\mathbf{r}_1+\mathbf{x}_2)\rho_3(\mathbf{r}_1+\mathbf{x}_3)\; V_{23}(\mathbf{x}_2,\mathbf{x}_3), \tag{14a}$$

$$V_{\rm SE,\,F}^{\rm 3N} = -{\rm Tr}_1{\rm Tr}_2{\rm Tr}_3 \int d\mathbf{r}_1 d\mathbf{x}_2 d\mathbf{x}_3 \; \rho_1(\mathbf{r}_1+\mathbf{x}_2,\mathbf{r}_1)\rho_2(\mathbf{r}_1,\mathbf{r}_1+\mathbf{x}_2)\rho_3(\mathbf{r}_1+\mathbf{x}_3)V_{23}(\mathbf{x}_2,\mathbf{x}_3)\; P_{12}^{\sigma\tau}$$
$$-\frac{1}{2}{\rm Tr}_1{\rm Tr}_2{\rm Tr}_3 \int d\mathbf{r}_1 d\mathbf{x}_2 d\mathbf{x}_3 \; \rho_1(\mathbf{r}_1)\rho_2(\mathbf{r}_1+\mathbf{x}_3,\mathbf{r}_1+\mathbf{x}_2)\rho_3(\mathbf{r}_1+\mathbf{x}_2,\mathbf{r}_1+\mathbf{x}_3)V_{23}(\mathbf{x}_2,\mathbf{x}_3)\; P_{23}^{\sigma\tau}, \tag{14b}$$

$$V_{\rm DE,\,F}^{\rm 3N} = {\rm Tr}_1{\rm Tr}_2{\rm Tr}_3 \int d\mathbf{r}_1 d\mathbf{x}_2 d\mathbf{x}_3 \; \rho_1(\mathbf{r}_1+\mathbf{x}_3,\mathbf{r}_1)\rho_2(\mathbf{r}_1,\mathbf{r}_1+\mathbf{x}_2)\rho_3(\mathbf{r}_1+\mathbf{x}_2,\mathbf{r}_1+\mathbf{x}_3)V_{23}(\mathbf{x}_2,\mathbf{x}_3)\; P_{23}^{\sigma\tau}P_{12}^{\sigma\tau}. \tag{14c}$$

As in the NN system, the Hartree term is already diagonal in each of the OBDMs. As such the Hartree term is evaluated exactly while DME expansions are performed on the two exchange terms.

III. CHIRAL POTENTIALS

We derive DME couplings by working up to N^{2}LO in the chiral expansion including $3N$ forces, both with and without the Δ. Specially optimized N^{2}LO forces [64,65] have recently been used with success in nuclear calculations of medium-mass nuclei by fine-tuning the predicted saturation properties through fitting to properties of selected nuclei up to oxygen. This approach is philosophically similar to the global refit we will perform for our functional after adding in finite-range chiral physics. The various diagrams that contribute to the chiral expansion at different orders are displayed in Fig. 1.

Up to NLO, the chiral potentials depend on the pion mass m_π, the $\Delta-N$ mass splitting $M_{\Delta-N}$, the pion decay constant f_π, the nucleon axial vector coupling g_A, the N-to-Δ axial vector coupling h_A, and various NN contacts. For h_A, we use the large N_C value and adopt the convention of Ref. [66] to define it as $h_A = 3g_A/\sqrt{2}$. Note the factor of 2 difference compared to Ref. [67]. At N^{2}LO, the potentials further depend on the subleading LECs c_1, c_2, c_3, and c_4 derived from $\mathcal{L}_{\pi N}^{(2)}$, along with the subleading b_3+b_8 combination derived from $\mathcal{L}_{\pi N\Delta}^{(2)}$. The c_2 and b_3+b_8 LECs do not contribute to the potential in the Δ-less theory. The c_i LECs are unnaturally large in the Δ-less theory due to absorbing the contribution of the Δ isobar [68]. It is well known that this property weakens the NLO potential and causes the N^{2}LO potential to be unnaturally strong. The same effect happens for the $3N$ potential where the N^{3}LO contribution is small but the N^{4}LO term is large [69]. Including Δ isobars in the theory explicitly makes the c_i terms more natural, shifts more physics to NLO (N^{3}LO) for the NN ($3N$) potential, and improves the convergence of the chiral expansion. At N^{2}LO, the $3N$ potential additionally depends on an OPE contact term c_D and a $3N$ contact c_E.

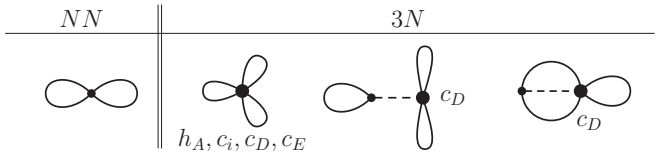

FIG. 2. Diagrams corresponding to the Hartree-Fock topologies absent in our DME couplings with all $3N$ vertices explicitly labeled. Notation is as in Fig. 1. Diagrams without a dashed line have no finite-range radial function.

In this paper, we *only* consider the finite-range part of the chiral potentials, with short-range contributions to be absorbed into a refit of Skyrme parameters. We omit from the DME couplings all pure contact terms in the coordinate space chiral potentials that carry Dirac δ functions in the relative distance variables. For the NN case, these contributions have the same structures at Hartree-Fock as the Skyrme contacts of the EDF. Due to the presence of two relative distance variables in the $3N$ case, contributions are classified into long-range (LR) parts with c_i or h_A vertices and no Dirac δ functions, intermediate-range (IR) parts with c_i, h_A, or c_D vertices and one Dirac δ function, and short-range (SR) parts with c_i, h_A, c_D, or c_E vertices and two Dirac δ functions. Our DME couplings include contributions from all of the LR terms along with all c_i and h_A IR terms. For the $3N$ case, there is not an exact correspondence between the omitted IR c_D terms and the EDF Skyrme contacts but for the present work we assume that these contributions can be approximately absorbed in the global refit. The omitted contributions to the DME couplings are shown in Fig. 2 with the $3N$ vertices explicitly labeled. In Secs. III A and III B we give the unregulated forms of the NN and $3N$ potentials in coordinate space. Regularization is then briefly discussed in Sec. III C.

A. NN forces

The coordinate space vacuum NN potential can be conveniently decomposed in spin-isospin space in a purely local form. Up to N^{2}LO in the chiral expansion, the NN potential can be written as scalar functions of the relative distance r multiplying various spin-isospin operators:

$$V^{NN}(\mathbf{r},\{\sigma\tau\}) = [V_C(r) + W_C(r)\,\boldsymbol{\tau}_1\cdot\boldsymbol{\tau}_2] + [V_S(r) + W_S(r)\,\boldsymbol{\tau}_1\cdot\boldsymbol{\tau}_2]\boldsymbol{\sigma}_1\cdot\boldsymbol{\sigma}_2 + [V_T(r) + W_T(r)\,\boldsymbol{\tau}_1\cdot\boldsymbol{\tau}_2]S_{12}(\hat{\mathbf{r}})\,, \quad (15)$$

where $r \equiv |\mathbf{r}|$, $S_{12}(\hat{\mathbf{r}})$ is the usual tensor operator,

$$S_{12}(\hat{\mathbf{r}}) = 3(\boldsymbol{\sigma}_1\cdot\hat{\mathbf{r}})(\boldsymbol{\sigma}_2\cdot\hat{\mathbf{r}}) - \boldsymbol{\sigma}_1\cdot\boldsymbol{\sigma}_2\,, \quad (16)$$

and $\boldsymbol{\sigma}_i$ ($\boldsymbol{\tau}_i$) is the spin (isospin) operator for particle i. The isoscalar and isovector form factors, V_i and W_i respectively, have central (C), spin (S), and tensor (T) components. Thus, in the operator basis of Eq. (15) for the NN potential, we only need to consider three spin operator structures,

$$\mathcal{J}_1 = 1, \quad (17a)$$

$$\mathcal{J}_2 = \boldsymbol{\sigma}_1\cdot\boldsymbol{\sigma}_2, \quad (17b)$$

$$\mathcal{J}_3 = S_{12}(\hat{\mathbf{r}}), \quad (17c)$$

and two isospin operators,

$$\mathcal{K}_1 = 1, \quad (18a)$$

$$\mathcal{K}_2 = \boldsymbol{\tau}_1\cdot\boldsymbol{\tau}_2. \quad (18b)$$

Deriving V^{NN} from χEFT using Weinberg power counting, the long-range form factors at LO are given by Ref. [66], with $x \equiv rm_\pi$,[2]

$$W_S^{(0)}(r) = \frac{m_\pi^3}{12\pi}\left(\frac{g_A}{2f_\pi}\right)^2\frac{e^{-x}}{x}, \quad (19a)$$

$$W_T^{(0)}(r) = \frac{m_\pi^3}{12\pi}\left(\frac{g_A}{2f_\pi}\right)^2\frac{e^{-x}}{x}\left(1+\frac{3}{x}+\frac{3}{x^2}\right), \quad (19b)$$

which is the familiar OPE potential without the Dirac δ function.

The form factors at NLO including only nucleons and pions are given by Ref. [66],

$$W_C^{(2)}(r) = \frac{m_\pi^5}{8\pi^3(2f_\pi)^4}\frac{1}{x^4}\left\{x\left[1+10g_A^2-g_A^4(23+4x^2)\right]K_0(2x) + \left[1+2g_A^2(5+2x^2)-g_A^4(23+12x^2)\right]K_1(2x)\right\}, \quad (20a)$$

$$V_S^{(2)}(r) = \frac{m_\pi^5}{2\pi^3}\left(\frac{g_A}{2f_\pi}\right)^4\frac{1}{x^4}[3xK_0(2x) + (3+2x^2)K_1(2x)], \quad (20b)$$

$$V_T^{(2)}(r) = -\frac{m_\pi^5}{8\pi^3}\left(\frac{g_A}{2f_\pi}\right)^4\frac{1}{x^4}[12xK_0(2x) + (15+4x^2)K_1(2x)], \quad (20c)$$

where $K_0(x)$ and $K_1(x)$ are modified Bessel functions of the second kind. The form factors at N^{2}LO including only nucleons and pions are given by [66]

$$V_C^{(3)}(r) = \frac{3}{2}\frac{g_A^2m_\pi^6}{(2f_\pi)^4\pi^2}\frac{e^{-2x}}{x^6}[2c_1x^2(1+x)^2 + c_3(6+12x+10x^2+4x^3+x^4)], \quad (21a)$$

$$W_S^{(3)}(r) = \frac{1}{3}\frac{g_A^2m_\pi^6}{(2f_\pi)^4\pi^2}\frac{e^{-2x}}{x^6}c_4(1+x)(3+3x+2x^2), \quad (21b)$$

$$W_T^{(3)}(r) = -\frac{1}{3}\frac{g_A^2m_\pi^6}{(2f_\pi)^4\pi^2}\frac{e^{-2x}}{x^6}c_4(1+x)(3+3x+x^2). \quad (21c)$$

[2]Note that the potentials in Ref. [66] use $F_\pi = 2f_\pi = 184.80$ MeV.

The potentials given above need to be regulated to tame the short-distance singularities before being inserted in the Schrödinger equation (see Sec. III C). We emphasize again that the potentials above correspond *only* to the long-range chiral potentials (excluding terms with Dirac δ functions); short-range contact terms in the EFT have not been included.

When including explicit Δ isobars in the EFT, additional diagrams appear at both NLO and N^{2}LO consisting of single- and double-Δ excitations. At both NLO and N^{2}LO, these additional parts of the potential contribute to all 6 form factors given in Eq. (15). The explicit form of these potentials with Δs are given in Ref. [66] and are written in the Supplemental Material [61] for completeness.

B. 3*N* forces

As in the NN sector, the $3N$ potentials here will be purely local and defined in coordinate space. A general local three-body force will include permutations with respect to three different subsystems,

$$V^{3\mathrm{N}} = V_{12} + V_{23} + V_{13}\ , \tag{22}$$

where a potential V_{ij} will depend in general on two relative distances related to the choice of subscripts and the spin-isospin of the three particles. That is,

$$V_{ij} \equiv V(\mathbf{r}_{ik},\mathbf{r}_{jk},\sigma_1,\tau_1,\sigma_2,\tau_2,\sigma_3,\tau_3), \quad \mathbf{r}_{ab} \equiv \mathbf{r}_a - \mathbf{r}_b. \tag{23}$$

It is only necessary to include one of the three terms in Eq. (22) due to the symmetry of our three-body potentials under subscript interchange; see Sec. II. As such, in the $3N$ potentials given below, we arbitrarily choose the $V_{23}(\mathbf{r}_{21},\mathbf{r}_{31},\{\sigma\tau\})$ piece such that our potentials will have no direct dependence on the relative distance coordinate $\mathbf{r}_{23}$. In anticipation of the $3N$ potentials below, we define the following dimensionless functions [70]:

$$Y(r) \equiv \frac{\exp[-m_\pi r]}{m_\pi r}, \tag{24a}$$

$$U(r) \equiv 1 + \frac{1}{m_\pi r}, \tag{24b}$$

$$T(r) \equiv 1 + \frac{3}{m_\pi r} + \frac{3}{(m_\pi r)^2}, \tag{24c}$$

denoting the Yukawa function $Y(r)$, scalar function $U(r)$, and singular tensor function $T(r)$.

The $3N$ force at NLO is zero in the Δ-less case but has a Fujita-Miyazawa term when including explicit Δs [67,71,72],

$$V_{3N}^{(2)} = \alpha_1^{(2)} V_{C,1} + \alpha_2^{(2)} V_{C,2} + \alpha_3^{(2)} V_{C,3}, \tag{25}$$

with both $\alpha_i^{(2)}$ and $V_{C,i}$ specified below. Conveniently, the potential here has the same structure as the TPE term appearing at N^{2}LO. At N^{2}LO the $3N$ force has the structure [67,72,73]:

$$V_{3N}^{(3)} = \alpha_1^{(3)} V_{C,1} + \alpha_2^{(3)} V_{C,2} + \alpha_3^{(3)} V_{C,3} + V_D + V_E, \tag{26}$$

where the $\alpha_i^{(3)} V_{C,i}$ are TPE terms, V_D is an OPE term, and V_E is a $3N$ contact. As mentioned already, for the purposes of calculating the DME couplings up to N^{2}LO, only the LR and IR $V_{C,i}$ terms (Fujita-Miyazawa and TPE) are included. The SR $V_{C,i}$ terms as well as the V_D and V_E potentials are assumed to be approximately accounted for by the refit Skyrme terms, so we do not list here these operator structures.

The NLO prefactors for the V_C terms are given by [67]

$$\alpha_1^{(2)} \equiv 0, \quad \alpha_2^{(2)} \equiv -\frac{h_A^2 m_\pi^6 g_A^2}{2592 f_\pi^4 \pi^2 M_{\Delta-N}},$$
$$\alpha_3^{(2)} \equiv \frac{h_A^2 m_\pi^6 g_A^2}{10368 f_\pi^4 \pi^2 M_{\Delta-N}}, \tag{27}$$

while the N^{2}LO V_C prefactors are [67]

$$\alpha_1^{(3)} \equiv \frac{c_1 m_\pi^6 g_A^2}{16 f_\pi^4 \pi^2}, \quad \alpha_2^{(3)} \equiv \frac{c_3 m_\pi^6 g_A^2}{288 f_\pi^4 \pi^2}, \quad \alpha_3^{(3)} \equiv \frac{c_4 m_\pi^6 g_A^2}{576 f_\pi^4 \pi^2}. \tag{28}$$

For the purposes of performing the DME, it is convenient to organize the V_C operator structures. First, we enumerate the spin-isospin structures. The full $V_{C,i}$ expressions including all contacts are given in the Supplemental Material [61]. The $V_{C,1}$ potential only has one spin operator, which is a tensor-like term,

$$\mathcal{S}_1 \equiv (\boldsymbol{\sigma}_2 \cdot \hat{\mathbf{x}}_2)(\boldsymbol{\sigma}_3 \cdot \hat{\mathbf{x}}_3), \tag{29}$$

where we have used the variable transformation in Eq. (13). The $V_{C,2}$ potential has one spin-spin term and various other tensor terms,

$$\mathcal{S}_2 \equiv \boldsymbol{\sigma}_2 \cdot \boldsymbol{\sigma}_3, \tag{30a}$$
$$\mathcal{S}_3 \equiv (\boldsymbol{\sigma}_2 \cdot \hat{\mathbf{x}}_2)(\boldsymbol{\sigma}_3 \cdot \hat{\mathbf{x}}_2), \tag{30b}$$
$$\mathcal{S}_4 \equiv (\boldsymbol{\sigma}_2 \cdot \hat{\mathbf{x}}_3)(\boldsymbol{\sigma}_3 \cdot \hat{\mathbf{x}}_3), \tag{30c}$$
$$\mathcal{S}_5 \equiv (\boldsymbol{\sigma}_2 \cdot \hat{\mathbf{x}}_2)(\boldsymbol{\sigma}_3 \cdot \hat{\mathbf{x}}_3)(\hat{\mathbf{x}}_2 \cdot \hat{\mathbf{x}}_3). \tag{30d}$$

The final $V_{C,3}$ potential has various spin cross products,

$$\mathcal{S}_6 \equiv \boldsymbol{\sigma}_1 \cdot (\boldsymbol{\sigma}_2 \times \boldsymbol{\sigma}_3), \tag{31a}$$
$$\mathcal{S}_7 \equiv (\boldsymbol{\sigma}_2 \cdot \hat{\mathbf{x}}_2)\, \hat{\mathbf{x}}_2 \cdot (\boldsymbol{\sigma}_3 \times \boldsymbol{\sigma}_1), \tag{31b}$$
$$\mathcal{S}_8 \equiv (\boldsymbol{\sigma}_3 \cdot \hat{\mathbf{x}}_3)\, \hat{\mathbf{x}}_3 \cdot (\boldsymbol{\sigma}_1 \times \boldsymbol{\sigma}_2), \tag{31c}$$
$$\mathcal{S}_9 \equiv (\boldsymbol{\sigma}_2 \cdot \hat{\mathbf{x}}_2)(\boldsymbol{\sigma}_3 \cdot \hat{\mathbf{x}}_3)\, \boldsymbol{\sigma}_1 \cdot (\hat{\mathbf{x}}_2 \times \hat{\mathbf{x}}_3). \tag{31d}$$

There are only two isospin operators, one for the $V_{C,1}$, $V_{C,2}$ potentials and one for the $V_{C,3}$ potential,

$$\mathcal{T}_1 \equiv \boldsymbol{\tau}_2 \cdot \boldsymbol{\tau}_3, \tag{32a}$$
$$\mathcal{T}_2 \equiv \boldsymbol{\tau}_1 \cdot (\boldsymbol{\tau}_2 \times \boldsymbol{\tau}_3). \tag{32b}$$

The $V_{C,i}$ operator structures can then be written in terms of $\mathcal{S}$ and $\mathcal{T}$ [70,74],

$$V_{C,1} = \mathcal{T}_1\{\mathcal{S}_1\ \ \mathcal{Y}_1\}, \tag{33}$$

$$V_{C,2} = \mathcal{T}_1 \left\{ \begin{array}{l} \mathcal{S}_2(\mathcal{Y}_2 + \mathcal{Y}_{c,2}(x_2)\delta^3(\mathbf{x}_3) + \mathcal{Y}_{c,2}(x_3)\delta^3(\mathbf{x}_2)) \\ \quad +\mathcal{S}_3(\mathcal{Y}_3 + \mathcal{Y}_{c,3}(x_2)\delta^3(\mathbf{x}_3)) \\ \quad +\mathcal{S}_4(\mathcal{Y}_4 + \mathcal{Y}_{c,4}(x_3)\delta^3(\mathbf{x}_2)) \\ \quad +\mathcal{S}_5\mathcal{Y}_5 \end{array} \right\}, \tag{34}$$

$$V_{C,3} = \mathcal{T}_2 \left\{ \begin{array}{l} \mathcal{S}_6(\mathcal{Y}_6 + \mathcal{Y}_{c,6}(x_2)\delta^3(\mathbf{x}_3) + \mathcal{Y}_{c,6}(x_3)\delta^3(\mathbf{x}_2)) \\ \quad +\mathcal{S}_7(\mathcal{Y}_7 + \mathcal{Y}_{c,7}(x_2)\delta^3(\mathbf{x}_3)) \\ \quad +\mathcal{S}_8(\mathcal{Y}_8 + \mathcal{Y}_{c,8}(x_3)\delta^3(\mathbf{x}_2)) \\ \quad +\mathcal{S}_9\mathcal{Y}_9 \end{array} \right\}, \tag{35}$$

where the $\mathcal{Y}$ functions describe the radial dependence of the long-range physics associated with each spin operator. The $\mathcal{Y}_i(x_2,x_3)$ functions are explicitly given by

$$\mathcal{Y}_1 = U(x_2)Y(x_2)U(x_3)Y(x_3), \tag{36a}$$
$$\mathcal{Y}_2 = \mathcal{Y}_6 = [1 - T(x_2)][1 - T(x_3)]Y(x_2)Y(x_3), \tag{36b}$$
$$\mathcal{Y}_3 = \mathcal{Y}_7 = 3T(x_2)[1 - T(x_3)]Y(x_2)Y(x_3), \tag{36c}$$
$$\mathcal{Y}_4 = \mathcal{Y}_8 = 3T(x_3)[1 - T(x_2)]Y(x_2)Y(x_3), \tag{36d}$$
$$\mathcal{Y}_5 = \mathcal{Y}_9 = 9Y(x_2)Y(x_3)T(x_2)T(x_3). \tag{36e}$$

The $\mathcal{Y}_{c,i}(x)$ functions multiplying the contacts are given by

$$\mathcal{Y}_{c,2} = \mathcal{Y}_{c,6} = -\frac{4\pi}{m_\pi^3}[1 - T(x)]Y(x), \tag{37a}$$

$$\mathcal{Y}_{c,3} = \mathcal{Y}_{c,4} = \mathcal{Y}_{c,7} = \mathcal{Y}_{c,8} = -\frac{12\pi}{m_\pi^3}T(x)Y(x). \tag{37b}$$

Note that in all cases, we have matched the index of the $\mathcal{Y}$ functions to the associated spin operator for clarity. For later use, we also define $\mathcal{B}$ functions that incorporate the chiral prefactor associated with each potential,

$$\begin{aligned} \mathcal{B}_1 &\equiv \mathcal{Y}_1\alpha_1, \\ \mathcal{B}_i &\equiv \mathcal{Y}_i\alpha_2 \quad i \in \{2,3,4,5\}, \\ \mathcal{B}_i &\equiv \mathcal{Y}_i\alpha_3 \quad i \in \{6,7,8,9\}, \end{aligned} \tag{38}$$

$$\begin{aligned} \mathcal{B}_{c,i} &\equiv \mathcal{Y}_{c,i}\alpha_2 \quad i \in \{2,3,4\}, \\ \mathcal{B}_{c,i} &\equiv \mathcal{Y}_{c,i}\alpha_3 \quad i \in \{6,7,8\}. \end{aligned} \tag{39}$$

C. Regularization

The potentials above are calculated perturbatively from the chiral expansion with all divergences usually regulated with dimensional regularization. However, when they are iterated in the Schrödinger or Lippmann-Schwinger equation, an additional cutoff regularization scheme is required. For our NN potentials, each form factor $V_i(r)$, $W_i(r)$ is multiplied by a regulator function $f(r/R)$, where R is the cutoff [60]:

$$f\left(\frac{r}{R}\right) = \left[1 - \exp\left(-\frac{r^2}{R^2}\right)\right]^n. \tag{40}$$

This ensures that the long-range physics ($r \gg R$) is unsuppressed while the short-range parts of the potential ($r \ll R$) are cut off. This is only one possible form of the regulator in coordinate space; e.g., see Refs. [54,55]. Typical values used are $R = 0.8$–1.2 fm and $n = 4$–6. For $3N$ potentials, we use the same regulator function, including it as a part of each Yukawa function $Y(r)$. So after regularization, the finite-range chiral potentials are modified in the following manner:

$$V_i(r) \xrightarrow{\text{reg.}} V_i(r)\, f\left(\frac{r}{R_{NN}}\right) \quad \text{for } NN, \tag{41a}$$
$$W_i(r) \xrightarrow{\text{reg.}} W_i(r)\, f\left(\frac{r}{R_{NN}}\right) \quad \text{for } NN, \tag{41b}$$
$$Y(r) \xrightarrow{\text{reg.}} Y(r)\, f\left(\frac{r}{R_{3N}}\right) \quad \text{for } 3N, \tag{41c}$$

where we allow for the NN and $3N$ potentials to have two different values for the cutoff, R_{NN} and R_{3N}, respectively.

IV. EDF TECHNOLOGY

A. Local densities

Here we define the basic variables we will be working with in our Skyrme-like EDF. The OBDM can be decomposed into scalar-isoscalar, scalar-isovector, vector-isoscalar, and vector-isovector channels respectively [75,76]:

$$\begin{aligned} \rho(\mathbf{x},\mathbf{y}) &= \tfrac{1}{4}[\rho_0(\mathbf{x},\mathbf{y}) + \rho_1(\mathbf{x},\mathbf{y})\tau^z + \mathbf{s}_0(\mathbf{x},\mathbf{y})\cdot\boldsymbol{\sigma} \\ &\quad + \mathbf{s}_1(\mathbf{x},\mathbf{y})\cdot\boldsymbol{\sigma}\tau^z] \\ &= \tfrac{1}{4}[\rho_t(\mathbf{x},\mathbf{y}) + \mathbf{s}_t(\mathbf{x},\mathbf{y})\cdot\boldsymbol{\sigma}][\delta^{t,0} + \delta^{t,1}\tau^z]\,, \end{aligned} \tag{42}$$

where, by using τ_z instead of $\boldsymbol{\tau}$, we have assumed the OBDM is diagonal in isospin space. For time-reversal invariant systems, the scalar and vector OBDMs have the symmetry

$$\rho_t(\mathbf{x},\mathbf{y}) = \rho_t(\mathbf{y},\mathbf{x})\,, \quad \mathbf{s}_t(\mathbf{x},\mathbf{y}) = -\mathbf{s}_t(\mathbf{y},\mathbf{x})\,. \tag{43}$$

Our functional is built from a set of local densities including up to two derivatives [1]. Enumerating the different possibilities with derivatives acting on the scalar $\rho(\mathbf{r},\mathbf{r}')$ or vector $\mathbf{s}(\mathbf{r},\mathbf{r}')$ part of the OBDM, we get

$$\rho_t(\mathbf{r}) = \rho_t(\mathbf{r},\mathbf{r}')|_{\mathbf{r}=\mathbf{r}'}\,, \tag{44a}$$
$$s_{a,t}(\mathbf{r}) = s_{a,t}(\mathbf{r},\mathbf{r}')|_{\mathbf{r}=\mathbf{r}'}\,, \tag{44b}$$
$$\tau_t(\mathbf{r}) = \boldsymbol{\nabla}\cdot\boldsymbol{\nabla}'\rho_t(\mathbf{r},\mathbf{r}')|_{\mathbf{r}=\mathbf{r}'}\,, \tag{44c}$$
$$T_{a,t}(\mathbf{r}) = \boldsymbol{\nabla}\cdot\boldsymbol{\nabla}' s_{a,t}(\mathbf{r},\mathbf{r}')|_{\mathbf{r}=\mathbf{r}'}\,, \tag{44d}$$
$$j_{a,t}(\mathbf{r}) = -\frac{i}{2}(\boldsymbol{\nabla}_a - \boldsymbol{\nabla}'_a)\rho_t(\mathbf{r},\mathbf{r}')|_{\mathbf{r}=\mathbf{r}'}\,, \tag{44e}$$
$$J_{ab,t}(\mathbf{r}) = -\frac{i}{2}(\boldsymbol{\nabla}_a - \boldsymbol{\nabla}'_a)s_{b,t}(\mathbf{r},\mathbf{r}')|_{\mathbf{r}=\mathbf{r}'}\,, \tag{44f}$$

where we have defined the matter density ρ, spin density $\mathbf{s}$, kinetic density τ, spin-kinetic density $\mathbf{T}$, current density $\mathbf{j}$, and spin-current density $\mathbf{J}$. The subscript t denotes either isoscalar ($t = 0$) or isovector ($t = 1$) densities. Isoscalar and isovector quantities are defined to be either the sum or difference of neutron and proton densities, i.e.,

$$\rho_0(\mathbf{r}) \equiv \rho_n(\mathbf{r}) + \rho_p(\mathbf{r})\,, \quad \rho_1(\mathbf{r}) \equiv \rho_n(\mathbf{r}) - \rho_p(\mathbf{r})\,. \tag{45}$$

Note that ρ, τ, and $\mathbf{J}$ are time-even while $\mathbf{s}$, $\mathbf{T}$, and $\mathbf{j}$ are time-odd. Here, we restrict ourselves to time-reversal invariant systems such that all time-odd densities vanish. Therefore, for a first application, our results will only be applicable to even-even nuclei, which have time-reversal symmetry.

B. EDF form

The finite-range physics associated with pion exchange and Δ excitations are encoded as density-dependent couplings $g(\mathbf{R})$ in our EDF. The couplings $g(\mathbf{R})$ multiply various products of local densities and are added to the standard Skyrme functionals such that, e.g.,

$$U_t^{\rho\rho} \equiv g_t^{\rho\rho}(\mathbf{R}) + C_t^{\rho\rho} \,, \tag{46}$$

where U is the new coupling term and C is a standard term appearing in the Skyrme functional. For an NN potential given by Eq. (15), the EDF that results after performing the DME for the Fock term will consist of 12 bilinears of local densities with the form

$$V_{\rm F} \approx \sum_{t=0}^{1} \int d\mathbf{R}\; g_t^{\rho\rho}\rho_t\rho_t + g_t^{\rho\tau}\rho_t\tau_t + g_t^{\rho\Delta\rho}\rho_t\Delta\rho_t + g_t^{JJ,1}J_{t,aa}J_{t,bb} + g_t^{JJ,2}J_{t,ab}\,J_{t,ab} + g_t^{JJ,3}J_{t,ab}\,J_{t,ba} \,. \tag{47}$$

This is the same form as the EDF given in Ref. [20], modulo the spin-orbit contributions arising from the short-range NN contact interaction. For our $3N$ potentials, the resulting EDF for the Fock term will consist of 23 trilinears of local densities with the form

$$\begin{aligned} V_{\rm F} \approx \int d\mathbf{R}\; & g^{\rho_0^3}\rho_0^3 + g^{\rho_0^2\tau_0}\rho_0^2\tau_0 + g^{\rho_0^2\Delta\rho_0}\rho_0^2\Delta\rho_0 + g^{\rho_0(\nabla\rho_0)^2}\rho_0\nabla\rho_0\cdot\nabla\rho_0 + g^{\rho_0\rho_1^2}\rho_0\rho_1^2 + g^{\rho_1^2\tau_0}\rho_1^2\tau_0 + g^{\rho_1^2\Delta\rho_0}\rho_1^2\Delta\rho_0 \\ & + g^{\rho_0\rho_1\tau_1}\rho_0\rho_1\tau_1 + g^{\rho_0\rho_1\Delta\rho_1}\rho_0\rho_1\Delta\rho_1 + g^{\rho_0(\nabla\rho_1)^2}\rho_0\nabla\rho_1\cdot\nabla\rho_1 + \rho_0\epsilon_{ijk}[g^{\rho_0\nabla\rho_0 J_0}\nabla_i\rho_0 J_{0,jk} + g^{\rho_0\nabla\rho_1 J_1}\nabla_i\rho_1 J_{1,jk}] \\ & + \rho_1\epsilon_{ijk}[g^{\rho_1\nabla\rho_1 J_0}\nabla_i\rho_1 J_{0,jk} + g^{\rho_1\nabla\rho_0 J_1}\nabla_i\rho_0 J_{1,jk}] + \rho_0\big[g^{\rho_0 J_0^2,1}J_{0,aa}J_{0,bb} + g^{\rho_0 J_0^2,2}J_{0,ab}J_{0,ab} + g^{\rho_0 J_0^2,3}J_{0,ab}J_{0,ba}\big] \\ & + \rho_0\big[g^{\rho_0 J_1^2,1}J_{1,aa}J_{1,bb} + g^{\rho_0 J_1^2,2}J_{1,ab}J_{1,ab} + g^{\rho_0 J_1^2,3}J_{1,ab}J_{1,ba}\big] \\ & + \rho_1[g^{\rho_1 J_0 J_1,1}J_{1,aa}J_{0,bb} + g^{\rho_1 J_0 J_1,2}J_{1,ab}J_{0,ab} + g^{\rho_1 J_0 J_1,3}J_{1,ab}J_{0,ba}]. \end{aligned} \tag{48}$$

Our EDF above is similar to the one in Ref. [22], though more general as we have not assumed spherical symmetry for the self-consistent solutions. Also, the DME parametrization we adopt below in Sec. IV C is not identical to the one used in Ref. [22].

C. DME parametrization

There are three steps in applying the DME to derive couplings:

(1) perform spin-isospin traces on the operators present in the potential;
(2) expand the resulting OBDM structures using the DME;
(3) combine as needed the local densities, DME functions, and potentials for each coupling term and numerically perform the relevant integrals.

When performing the NN DME, nondiagonal OBDMs are expanded about the diagonal such that the nonlocality is factorized using the following formulas:

$$\rho_t\left(\mathbf{R}+\frac{\mathbf{r}}{2},\mathbf{R}-\frac{\mathbf{r}}{2}\right) \approx \sum_{n=0}^{n_{\rm max}} \Pi_n^{\rho}(kr)\mathcal{P}_n(\mathbf{R}) \,, \tag{49}$$

$$\mathbf{s}_t\left(\mathbf{R}+\frac{\mathbf{r}}{2},\mathbf{R}-\frac{\mathbf{r}}{2}\right) \approx \sum_{m=0}^{m_{\rm max}} \Pi_m^{s}(kr)\mathcal{Q}_m(\mathbf{R}) \,, \tag{50}$$

where the Π functions are specified by the DME variant and $\mathcal{P}_n(\mathbf{R})$, $\mathcal{Q}_m(\mathbf{R})$ denote various local densities. The momentum scale k in the Π functions sets the scale for falloff in the off-diagonal direction of the OBDM; one is free to choose k in such a way that the expansion is optimized. We define the momentum scale k to be the local Fermi momentum,

$$k \equiv k_{\rm F}(\mathbf{R}) = \left(\frac{3\pi^2}{2}\rho_0(\mathbf{R})\right)^{1/3}, \tag{51}$$

where ρ_0 is the isoscalar density. However, alternative choices of k, for example, involving $\tau(\mathbf{R})$ and $\Delta\rho(\mathbf{R})$, are also possible [77].

We follow past practice and truncate the DME expansion at $n_{\rm max} = 2$ and $m_{\rm max} = 1$ such that

$$\rho\left(\mathbf{R}+\frac{\mathbf{r}}{2},\mathbf{R}-\frac{\mathbf{r}}{2}\right) \approx \Pi_0^{\rho}(k_{\rm F}r)\rho(\mathbf{R}) + \frac{r^2}{6}\Pi_2^{\rho}(k_{\rm F}r) \times\left[\frac{1}{4}\Delta\rho(\mathbf{R}) - \tau(\mathbf{R}) + \frac{3}{5}k_{\rm F}^2\rho(\mathbf{R})\right], \tag{52}$$

$$s_b\left(\mathbf{R}+\frac{\mathbf{r}}{2},\mathbf{R}-\frac{\mathbf{r}}{2}\right) \approx i\,\Pi_1^{s}(k_{\rm F}r)\sum_{a=x}^{z} r_a J_{ab}(\mathbf{R}). \tag{53}$$

The DME parametrization we adopt is the simplified phase-space-averaging (PSA) [20,21] choice, which was shown to better reproduce the vector part of the OBDM over the original Negele-Vautherin prescription. For this choice, the Π functions are given by

$$\Pi_0^{\rho}(k_{\rm F}x) = \Pi_2^{\rho}(k_{\rm F}x) = \Pi_1^{s}(k_{\rm F}x) = 3\frac{j_1(k_{\rm F}x)}{k_{\rm F}x} \,, \tag{54}$$

where j_1 is a spherical Bessel function of the first kind. Applying the symmetry principle in Eq. (43), the DME expansion can also be applied to OBDMs with reversed arguments.

For the three-body system, as anticipated by the transformation to Eq. (14), a different set of coordinates than

the center-of-mass choice is needed. A successful coordinate choice for the DME allows for factorization of the variable appearing in the local densities and the variables appearing in the potential and DME Π functions. For the three-body system, these conditions can be satisfied by performing the DME expansion about the location of one of the particles, i.e., $\mathbf{r}_1$ in Eq. (14). However, this choice of coordinates leads to OBDMs with two nonlocality coordinates in some cases; this is in contrast to the one nonlocality variable that occurs in two-body systems. Assessing the ultimate accuracy of the simplified PSA-DME in such cases is an open research topic. In the following, we follow the straightforward generalization articulated in Ref. [63]. For the scalar part of the OBDM, this leads to the following DME expansion equations [63]:

$$\begin{aligned}&\rho(\mathbf{r}_1,\mathbf{r}_1+\mathbf{x})\\&\quad\approx \Pi_0^{\rho}(k_{\rm F}x)\rho(\mathbf{r}_1)\\&\qquad+\frac{x^2}{6}\Pi_2^{\rho}(k_{\rm F}x)\left[\frac{1}{2}\Delta\rho(\mathbf{r}_1)-\tau(\mathbf{r}_1)+\frac{3}{5}k_{\rm F}^2\rho(\mathbf{r}_1)\right],\end{aligned}\tag{55}$$

$$\begin{aligned}&\rho(\mathbf{r}_1+\mathbf{x}_2,\mathbf{r}_1+\mathbf{x}_3)\\&\quad\approx \Pi_0^{\rho}(k_{\rm F}l)\left[\rho(\mathbf{r}_1)+\mathbf{N}\cdot\nabla\rho(\mathbf{r}_1)+\frac{1}{2}(\mathbf{N}\cdot\nabla)^2\rho(\mathbf{r}_1)\right]\\&\qquad+\frac{l^2}{6}\Pi_2^{\rho}(k_{\rm F}l)\left[\gamma\,\Delta\rho(\mathbf{r}_1)-\tau(\mathbf{r}_1)+\frac{3}{5}k_{\rm F}^2\rho(\mathbf{r}_1)\right],\end{aligned}\tag{56}$$

where

$$\mathbf{l}\equiv\mathbf{x}_2-\mathbf{x}_3,\quad \mathbf{N}\equiv(1-a)\mathbf{x}_2+a\mathbf{x}_3,\quad \gamma\equiv a^2-a+1/2.\tag{57}$$

The variable a reflects our freedom in choosing how to perform the DME expansion with respect to the 23 particle subsystem. For the choice $a=1/2$, the usual center-of-mass choice is recovered. For the vector part, the expansion equations are [63]

$$s_b(\mathbf{r}_1+\mathbf{x},\mathbf{r}_1)\approx i\,\Pi_1^{s}(k_{\rm F}x)\sum_{a=x}^{z}x_a\;J_{ab}(\mathbf{r}_1),\tag{58}$$

$$s_b(\mathbf{r}_1+\mathbf{x}_2,\mathbf{r}_1+\mathbf{x}_3)\approx i\,\Pi_1^{s}(k_{\rm F}l)\sum_{a=x}^{z}l_a\;J_{ab}(\mathbf{r}_1).\tag{59}$$

For the expansions in Eqs. (55), (56), (58), and (59), the Π functions are again given by Eq. (54). As before, DME expansions for OBDMs with reversed arguments can be found using Eq. (43). In the Supplemental Material [61] we show an example of how these expansions are performed.

V. DME FOR *NN* FORCES

Because we do not plan to apply the DME to the Hartree term, we concentrate only on the exchange term. The Fock energy is given by

$$\begin{aligned}V_{\rm F}=-\frac{1}{2}{\rm Tr}_1{\rm Tr}_2\int d\mathbf{R}\,d\mathbf{r}\;\rho_1\left(\mathbf{R}-\frac{\mathbf{r}}{2},\mathbf{R}+\frac{\mathbf{r}}{2}\right)\\\times\rho_2\left(\mathbf{R}+\frac{\mathbf{r}}{2},\mathbf{R}-\frac{\mathbf{r}}{2}\right)V^{\rm NN}(\mathbf{r},\{\sigma\tau\})P_{12}^{\sigma\tau}.\end{aligned}\tag{60}$$

Note that in applying Eqs. (49) and (50) to the Fock energy, the integrations over $\mathbf{R}$ and $\mathbf{r}$ will factorize. The $\mathbf{r}$ integral will go over the Π functions and $V^{\rm NN}$ while the $\mathbf{R}$ integral will be the remaining integral in the EDF of Eq. (47). Equation (60) can be rendered in a more compact form via

$$V_{\rm F}=-\frac{1}{2}\sum_{ij}\int d\mathbf{R}\,d\mathbf{r}A_iB_j\widetilde{V}(r)_{ij},\tag{61}$$

where $\widetilde{V}(r)_{ij}$ is an isoscalar or isovector form factor from Eq. (15) with pure radial dependence, and the large Latin letters include information about the spin-isospin traces:

$$A_m=\frac{1}{4}\prod_{i=1}^{2}{\rm Tr}_{\sigma_i}\left[(\rho_{t,i}(\mathbf{a}_i)+\mathbf{s}_{t,i}(\mathbf{a}_i)\cdot\boldsymbol{\sigma}_i)\,\mathcal{J}_m\,P_{12}^{\sigma}\right],\tag{62a}$$

$$B_m=\frac{1}{4}\prod_{i=1}^{2}{\rm Tr}_{\tau_i}\left[\left(\delta_i^{t,0}+\delta_i^{t,1}\tau_i^z\right)\mathcal{K}_m\,P_{12}^{\tau}\right].\tag{62b}$$

Note that in Eq. (62), the OBDMs have been decomposed into scalar and vector parts with the isospin part factorized by Eq. (42). The $\mathbf{a}$ variables are schematic stand-ins for the arguments of the OBDMs appearing in Eq. (60), and $\mathcal{J}_m$ and $\mathcal{K}_m$ are, respectively, the spin and isospin operators in Eqs. (17) and (18). Now, we follow the steps outlined in Sec. IV C.

A. *NN* DME step 1: Traces

Inserting the $\mathcal{J}$ and $\mathcal{K}$ operators into Eqs. (62a) and (62b) and evaluating the traces yields

$$A_1=\tfrac{1}{2}(\rho_1\;\rho_2+\mathbf{s}_1\cdot\mathbf{s}_2),\tag{63a}$$

$$A_2=\tfrac{1}{2}(3\rho_1\;\rho_2-\mathbf{s}_1\cdot\mathbf{s}_2),\tag{63b}$$

$$A_3=3(\mathbf{s}_1\cdot\hat{\mathbf{r}})(\mathbf{s}_2\cdot\hat{\mathbf{r}})-\mathbf{s}_1\cdot\mathbf{s}_2,\tag{63c}$$

and

$$B_1=\tfrac{1}{2}\left(\delta_1^{t,0}\;\delta_2^{t,0}+\delta_1^{t,1}\;\delta_2^{t,1}\right),\tag{64a}$$

$$B_2=\tfrac{1}{2}\left(3\delta_1^{t,0}\;\delta_2^{t,0}-\delta_1^{t,1}\;\delta_2^{t,1}\right),\tag{64b}$$

where the arguments of the scalar (ρ) and vector ($\mathbf{s}$) density matrices along with the isoscalar or isovector subscript t have been suppressed for brevity.

B. *NN* DME step 2: DME dictionary

Looking at the elements in Eq. (63), it is apparent that a DME expansion needs to be performed on only three unique OBDM structures:

$$\{\rho_1\;\rho_2,\quad \mathbf{s}_1\cdot\mathbf{s}_2,\quad (\mathbf{s}_1\cdot\hat{\mathbf{r}})(\mathbf{s}_2\cdot\hat{\mathbf{r}})\}.\tag{65}$$

Below, we apply the DME parametrization defined in Sec. IV C and keep terms up to second order. The format for the DME expansions given below has scalar or vector density matrices on the left and local densities on the right:

$$\text{scalar or vector density matrices}\xrightarrow{\rm DME}\left\{\text{local densities}\times\text{DME expression}\right\},$$

where the DME expression on the right-hand side has had all nonlocal variable integrals done except for the relative distance magnitude r. Below, we restore the spatial dependence in the OBDMs and local densities for clarity. The expanded structures are given by

$$\rho_1\left(\mathbf{R}-\frac{\mathbf{r}}{2},\mathbf{R}+\frac{\mathbf{r}}{2}\right)\rho_2\left(\mathbf{R}+\frac{\mathbf{r}}{2},\mathbf{R}-\frac{\mathbf{r}}{2}\right)\xrightarrow{\text{DME}}\begin{Bmatrix}\rho_1(\mathbf{R})\rho_2(\mathbf{R}) & \mathcal{O}_1\\ +\rho_1(\mathbf{R})\tau_2(\mathbf{R}) & \mathcal{O}_2\\ +\tau_1(\mathbf{R})\rho_2(\mathbf{R}) & \mathcal{O}_2\\ +\rho_1(\mathbf{R})\Delta\rho_2(\mathbf{R}) & \mathcal{O}_3\\ +\Delta\rho_1(\mathbf{R})\rho_2(\mathbf{R}) & \mathcal{O}_3\end{Bmatrix}, \tag{66}$$

$$\mathbf{s}_1\left(\mathbf{R}-\frac{\mathbf{r}}{2},\mathbf{R}+\frac{\mathbf{r}}{2}\right)\cdot\mathbf{s}_2\left(\mathbf{R}+\frac{\mathbf{r}}{2},\mathbf{R}-\frac{\mathbf{r}}{2}\right)\xrightarrow{\text{DME}}\begin{Bmatrix}J_{1,ab}(\mathbf{R})J_{2,ab}(\mathbf{R}) & \mathcal{O}_4\end{Bmatrix}, \tag{67}$$

$$\mathbf{s}_1\left(\mathbf{R}-\frac{\mathbf{r}}{2},\mathbf{R}+\frac{\mathbf{r}}{2}\right)\cdot\hat{\mathbf{r}}\,\mathbf{s}_2\left(\mathbf{R}+\frac{\mathbf{r}}{2},\mathbf{R}-\frac{\mathbf{r}}{2}\right)\cdot\hat{\mathbf{r}}\xrightarrow{\text{DME}}\begin{Bmatrix}J_{1,aa}(\mathbf{R})J_{2,bb}(\mathbf{R}) & \mathcal{O}_4/5\\ +J_{1,ab}(\mathbf{R})J_{2,ab}(\mathbf{R}) & \mathcal{O}_4/5\\ +J_{1,ab}(\mathbf{R})J_{2,ba}(\mathbf{R}) & \mathcal{O}_4/5\end{Bmatrix}, \tag{68}$$

where the $\mathcal{O}_i(r,k_\mathrm{F})$ functions, which contain the DME Π functions and relative distance dependence, are given by

$$\mathcal{O}_1=\left[\Pi_0^\rho(k_\mathrm{F}r)\right]^2+\frac{r^2k_\mathrm{F}^2}{5}\Pi_0^\rho(k_\mathrm{F}r)\Pi_2^\rho(k_\mathrm{F}r), \tag{69a}$$

$$\mathcal{O}_2=-\frac{r^2}{6}\Pi_0^\rho(k_\mathrm{F}r)\Pi_2^\rho(k_\mathrm{F}r), \tag{69b}$$

$$\mathcal{O}_3=\frac{r^2}{24}\Pi_0^\rho(k_\mathrm{F}r)\Pi_2^\rho(k_\mathrm{F}r), \tag{69c}$$

$$\mathcal{O}_4=\frac{r^2}{3}\left[\Pi_1^s(k_\mathrm{F}r)\right]^2. \tag{69d}$$

C. *NN* DME step 3: Couplings

Combining the different local densities in Eqs. (66)–(68) with the isospin traces in Eq. (64), one can verify the 12 different possible local density bilinears seen in Eq. (47). Using Eqs. (63) and (64) as input into Eq. (61) along with the DME dictionary, symbolic software can then perform the algebraic manipulations necessary to isolate the equations for each individual DME coupling such that we have an EDF of the form of Eq. (47). The coupling expressions are

$$g_t^{\rho\rho}(\mathbf{R})=-\frac{4\pi}{2}\int dr\,r^2\frac{1}{4}\mathcal{O}_1\;\Xi_t^1\,, \tag{70a}$$

$$g_t^{\rho\tau}(\mathbf{R})=-\frac{4\pi}{2}\int dr\,r^2\frac{1}{2}\mathcal{O}_2\;\Xi_t^1\,, \tag{70b}$$

$$g_t^{\rho\Delta\rho}(\mathbf{R})=-\frac{4\pi}{2}\int dr\,r^2\frac{1}{2}\mathcal{O}_3\;\Xi_t^1\,, \tag{70c}$$

$$g_t^{JJ,1}(\mathbf{R})=-\frac{4\pi}{2}\int dr\,r^2\frac{3}{10}\mathcal{O}_4\;\Xi_t^2\,, \tag{70d}$$

$$g_t^{JJ,2}(\mathbf{R})=-\frac{4\pi}{2}\int dr\,r^2\frac{1}{20}\mathcal{O}_4\;\Xi_t^3\,, \tag{70e}$$

$$g_t^{JJ,3}(\mathbf{R})=-\frac{4\pi}{2}\int dr\,r^2\frac{3}{10}\mathcal{O}_4\;\Xi_t^2\,, \tag{70f}$$

where the Ξ functions encapsulate the coupling dependence on the different potential form factors from Eq. (15),

$$\Xi_t^1=\begin{cases}V_C+3W_C+3V_S+9W_S & t=0,\\ V_C-W_C+3V_S-3W_S & t=1,\end{cases} \tag{71a}$$

$$\Xi_t^2=\begin{cases}V_T+3W_T & t=0,\\ V_T-W_T & t=1,\end{cases} \tag{71b}$$

$$\Xi_t^3=\begin{cases}5V_C+15W_C-5V_S-15W_S-4V_T-12W_T & t=0,\\ 5V_C-5W_C-5V_S+5W_S-4V_T+4W_T & t=1.\end{cases} \tag{71c}$$

VI. DME FOR 3*N* FORCES

Utilizing the organization of the V_C operators in Sec. III B, the exchange terms are rewritten as

$$V_{\mathrm{SE,F}}^{\mathrm{3N}}=-\sum_{jk}\int d\mathbf{r}_1d\mathbf{x}_2d\mathbf{x}_3\;C_j\;D_k\;\widetilde{V}_{23,jk}(x_2,x_3)$$
$$-\frac{1}{2}\sum_{jk}\int d\mathbf{r}_1d\mathbf{x}_2d\mathbf{x}_3\;E_j\;F_k\;\widetilde{V}_{23,jk}(x_2,x_3), \tag{72}$$

$$V_{\mathrm{DE,F}}^{\mathrm{3N}}=\sum_{jk}\int d\mathbf{r}_1d\mathbf{x}_2d\mathbf{x}_3\;G_j\;H_k\;\widetilde{V}_{23,jk}(x_2,x_3), \tag{73}$$

where the jk sum goes over all the spin-isospin operators in the potential, the large Latin letters refer to the result of traces, and $\widetilde{V}_{23,jk}(x_2,x_3)$ refers to the corresponding radial parts of the potential in the braces in in Eqs. (33)–(35), along with the correct chiral prefactor. The large Latin letters are given by

$$C_j=\frac{1}{8}\prod_{i=1}^{3}\mathrm{Tr}_{\sigma_i}\left[\left(\rho_{t,i}(\mathbf{a}_i)+\mathbf{s}_{t,i}(\mathbf{a}_i)\cdot\boldsymbol{\sigma}_i\right)\mathcal{S}_jP_{12}^\sigma\right], \tag{74a}$$

$$D_j=\frac{1}{8}\prod_{i=1}^{3}\mathrm{Tr}_{\tau_i}\left[\left(\delta_i^{t,0}+\delta_i^{t,1}\tau_i^z\right)\mathcal{T}_jP_{12}^\tau\right], \tag{74b}$$

$$E_j=\frac{1}{8}\prod_{i=1}^{3}\mathrm{Tr}_{\sigma_i}\left[\left(\rho_{t,i}(\mathbf{a}_i)+\mathbf{s}_{t,i}(\mathbf{a}_i)\cdot\boldsymbol{\sigma}_i\right)\mathcal{S}_jP_{23}^\sigma\right], \tag{74c}$$

$$F_j = \frac{1}{8}\prod_{i=1}^{3}\mathrm{Tr}_{\tau_i}\left[\left(\delta_i^{t,0}+\delta_i^{t,1}\tau_i^z\right)\mathcal{T}_j P_{23}^{\tau}\right], \tag{74d}$$

$$G_j = \frac{1}{8}\prod_{i=1}^{3}\mathrm{Tr}_{\sigma_i}\left[\left(\rho_{t,i}(\mathbf{a}_i)+\mathbf{s}_{t,i}(\mathbf{a}_i)\cdot\boldsymbol{\sigma}_i\right)\mathcal{S}_j P_{23}^{\sigma}P_{12}^{\sigma}\right], \tag{74e}$$

$$H_j = \frac{1}{8}\prod_{i=1}^{3}\mathrm{Tr}_{\tau_i}\left[\left(\delta_i^{t,0}+\delta_i^{t,1}\tau_i^z\right)\mathcal{T}_j P_{23}^{\tau}P_{12}^{\tau}\right], \tag{74f}$$

with the $\mathbf{a}_i$ schematically standing in for the pair of terms appearing in the OBDM in Eq. (14), the $1/8$ prefactor coming from pulling out the result of the traces,[3] and the $\mathcal{S}$, $\mathcal{T}$ terms specified by Eqs. (29)–(32). Again to derive coupling expressions, we follow the steps outlined in Sec. IV C.

A. 3N DME step 1: Traces

Here we explicitly do the traces for the six spin operator structures $\mathcal{S}_1$, $\mathcal{S}_2$, $\mathcal{S}_6$, $\mathcal{S}_7$, $\mathcal{S}_8$, and $\mathcal{S}_9$ along with $\mathcal{T}_1$ and $\mathcal{T}_2$. Operators $\mathcal{S}_3$, $\mathcal{S}_4$, and $\mathcal{S}_5$, follow from the trace of $\mathcal{S}_1$. After performing the spin traces, we then

(1) discard all terms with a local spin density, $\mathbf{s}(\mathbf{r})$, due to time-reversal invariance;
(2) discard terms with three vector densities as we restrict our EDF to second order in derivatives.

1. Hartree term

As previously mentioned, the OBDMs for the Hartree term are diagonal and the term can thus be evaluated exactly. However, as all of our $V_{C,i}$ three-body potentials in Eqs. (33)–(35) contain at least one Pauli spin matrix, the spin traces will yield at least one local spin density for each term. Therefore, the Hartree term will exactly vanish for time-reversal invariant systems.

Note also that the isospin traces over the operator $\mathcal{T}_2$ will identically vanish given isospin symmetry. As such, even for systems without time-reversal invariance, the $V_{C,3}$ potential will not contribute to the Hartree term assuming isospin is a good symmetry.

2. Single exchange traces

The single exchange part has two terms, one corresponding to P_{12} and another to P_{23}. Consulting Eq. (14), it is seen that the density matrix with subscript 3 for the first single exchange term will be diagonal as the P_{12} operator does not act upon it. However, all of the three-body potentials under consideration in Eqs. (33)–(35) contain a Pauli spin matrix $\boldsymbol{\sigma}_3$. After spin traces, this will yield a local spin density and thus vanish for time-reversal invariant systems:

$$C_i \longrightarrow 0 \quad \text{for all } i\ . \tag{75}$$

Likewise for the second part of the single exchange in Eq. (14), the density matrix with subscript 1 is diagonal.

TABLE I. Summary table for the various LECs and physical parameters appearing in our NN and $3N$ potentials up to N^{2}LO. For all potentials, $m_\pi = 138\,\mathrm{MeV}$, $f_\pi = 92.4\,\mathrm{MeV}$, and $g_A = 1.29$. In the table, $M_{\Delta-N}$ is given in MeV and h_A is dimensionless. The subleading c_is and the b_i combination are given in GeV^{-1}, and are taken from the fit to $\pi-N$ scattering data in Ref. [78].

	$M_{\Delta-N}$	h_A	c_1	c_2	c_3	c_4	b_3+b_8
Δ-less			−0.57	2.84	−3.87	2.89	
With Δs	293	2.74	−0.57	−0.25	−0.79	1.33	1.40

Because all terms of the $V_{C,3}$ potential in Eq. (35) have a $\boldsymbol{\sigma}_1$ Pauli spin matrix, all $V_{C,3}$ terms will yield a local spin density after traces. Therefore, this contribution will vanish for time-reversal invariant systems:

$$E_i \longrightarrow 0 \quad \text{for } i = 6,7,8,9\ . \tag{76}$$

The remaining nonzero single exchange spin and isospin traces, E_i and F_i respectively, are given in the Supplemental Material [61].

3. Double exchange traces

The double exchange traces are more involved due to the extra exchange operator and the fact that all of the spin operators have a nonzero contribution. The expressions for the spin and isospin traces, G_i and H_i respectively, are given in the Supplemental Material [61].

B. 3N DME step 2: DME dictionary

Due to its length, we relegate the DME dictionary for the single exchange and double exchange terms to the Supplemental Material [61]. The format for the DME expansions in these appendices is given schematically by

$$\text{density matrices} \xrightarrow{\text{DME}} \left\{\text{local densities} \times (\text{LR or IR DME expression})\right\}\ ,$$

where the LR DME expression has all integrals done except for the x_2, x_3 magnitudes and the relative angle θ between the two vectors. For the IR DME expression, only one integral over the magnitude of the nonlocality variable, generically called x, remains.

C. 3N DME step 3: Couplings

Again due to length, we relegate the final expressions of the $3N$ couplings to the Supplemental Material [61].[4]

VII. RESULTS

In this section, we show results for some representative examples of the NN and $3N$ couplings $g(\mathbf{R})$. Values of the various physical parameters and LECs used in these results

[3] For Eqs. (72) and (73), a factor of $1/4^3$ from expanding the OBDMs and 8^2 from the traces have been combined to give unity.

[4] The code used to calculate the $3N$ couplings is available upon request.

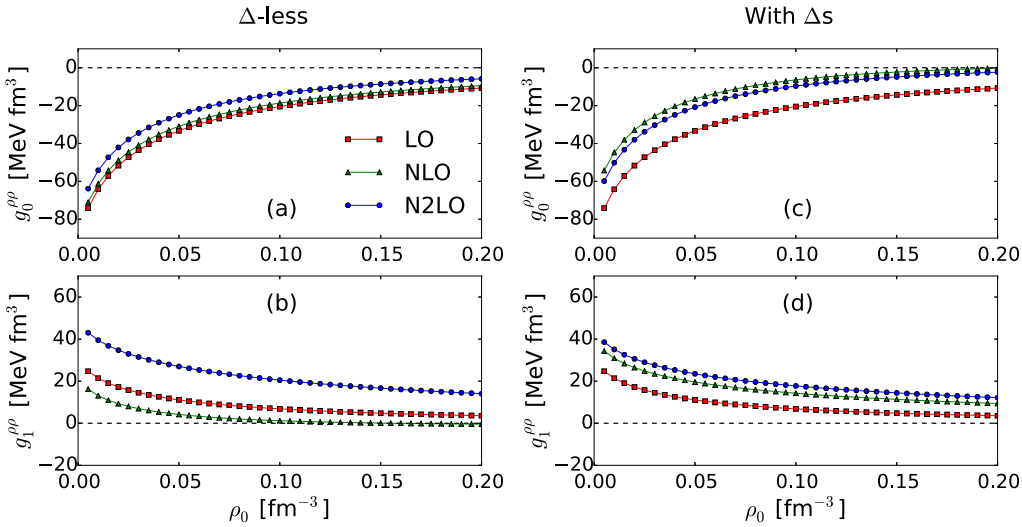

FIG. 3. The $g_t^{\rho\rho}$ couplings from Eq. (70a) are plotted as a function of the isoscalar density ρ_0 at fixed cutoff $R_{NN} = 1.2$ fm using the regulator in Eq. (40) with $n = 6$. The values for the couplings are shown at three different chiral orders up to N^{2}LO. The isoscalar coupling $g_0^{\rho\rho}$ is shown without (a) and with (c) Δ isobars. The isovector coupling $g_1^{\rho\rho}$ is shown without (b) and with (d) Δ isobars.

are given in Table I. The values of the subleading c_i LECs still have significant uncertainties, but we do not consider them in the present discussion. For an in-depth discussion on LEC values, see, e.g., Ref. [79]. In the NN sector, we examine the isoscalar and isovector coupling for the density-density term in Eq. (70a), $g_0^{\rho\rho}$ and $g_1^{\rho\rho}$ respectively. In Fig. 3, we plot these couplings as a function of the isoscalar density at a fixed cutoff $R_{NN} = 1.2$ fm using the regulator defined in Eq. (40). The coupling is shown for three different chiral orders up to N^{2}LO both with and without explicit Δ resonances. In Fig. 4, we show the same couplings but at a harder cutoff of $R_{NN} = 1.0$ fm.

In all cases, the variation of the couplings with density is largest in the low density regime, while at higher densities the couplings tend to asymptote at some finite value. This reflects the functional form of the DME Π functions used in Sec. IV C. The Π functions defined in Eq. (54) are largest at small arguments and have the greatest variation close to zero but die away as the argument increases. As the Π functions are finite in the limit $k_F \to 0$ and $k_F \to \infty$, the couplings are also well behaved in the same limits. Nevertheless, the enhancement of the couplings in the low density limit may necessitate a different fitting procedure. As an example, the couplings could be multiplied by the isoscalar density, $g_t^{\rho\rho} \to \rho_0 g_t^{\rho\rho}$, such that the very low density behavior is not biasing the functional fit.

As the cutoff R_{NN} is lowered from 1.2 to 1.0 fm, the coupling calculations at different orders tend to move around

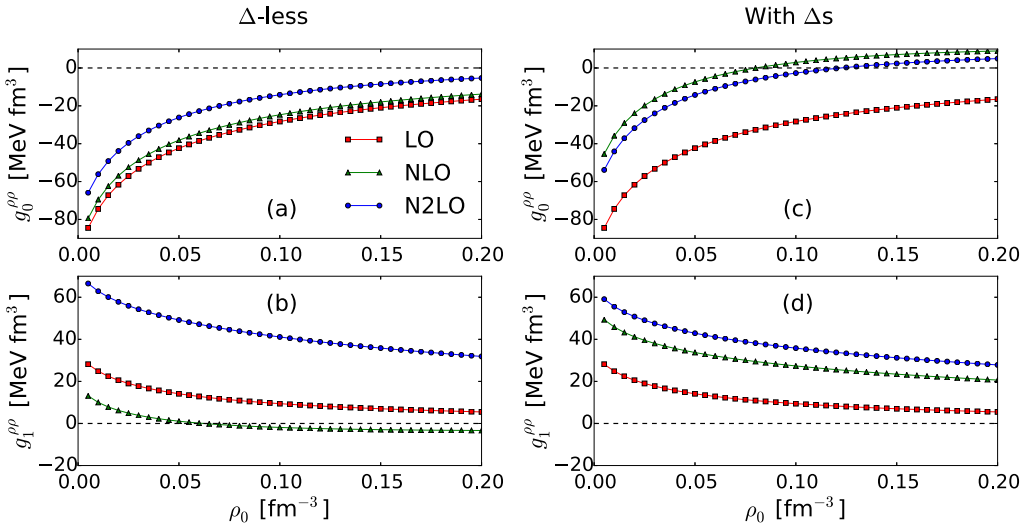

FIG. 4. The $g_t^{\rho\rho}$ couplings from Eq. (70a) are plotted as a function of the isoscalar density ρ_0 at fixed cutoff $R_{NN} = 1.0$ fm using the regulator in Eq. (40) with $n = 6$. The values for the couplings are shown at three different chiral orders up to N^{2}LO. The isoscalar coupling $g_0^{\rho\rho}$ is shown without (a) and with (c) Δ isobars. The isovector coupling $g_1^{\rho\rho}$ is shown without (b) and with (d) Δ isobars.

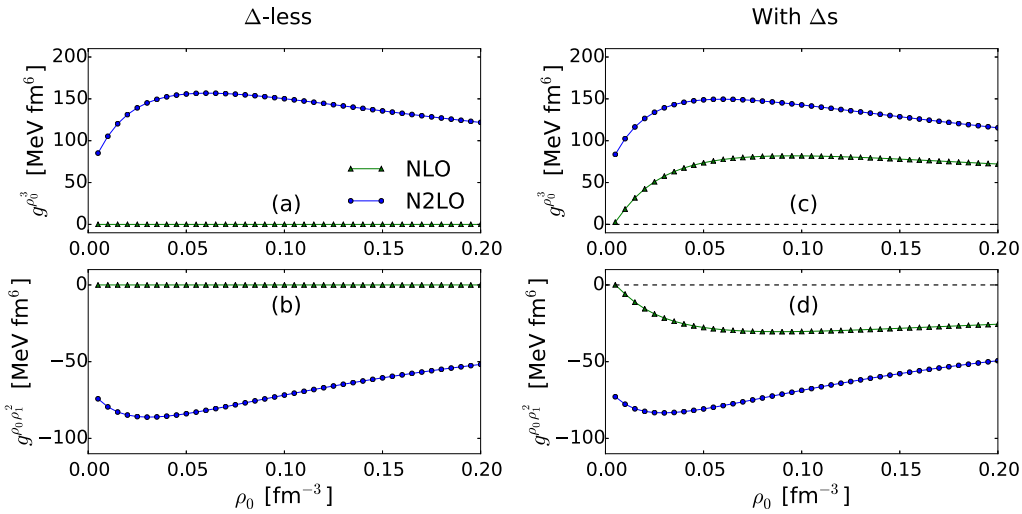

FIG. 5. The $g^{\rho_0^3}$ and $g^{\rho_0\rho_1^2}$ couplings are plotted as a function of the isoscalar density ρ_0 at fixed cutoff $R_{3N} = 1.2$ fm using the regulator in Eq. (40) with $n = 6$. The values for the couplings are shown at two different chiral orders up to N^{2}LO. The coupling $g^{\rho_0^3}$ is shown without (a) and with (c) Δ isobars. The coupling $g^{\rho_0\rho_1^2}$ is shown without (b) and with (d) Δ isobars.

and spread away from each other. This movement is most dramatic at NLO and N^{2}LO as these chiral potentials contain increasingly singular terms. However, over the range of the two cutoffs considered here, the N^{2}LO couplings vary by less than a factor of 2. These differences seen at different chiral orders and cutoffs is expected to be compensated for by a complementary shift in the Skyrme contacts after a global refit is performed.

Comparing the Δ-less and the implementation with Δs, the LO couplings between the two are equivalent as the Δ does not contribute at this order. Going to higher orders, there is a stark difference between the two at NLO which is partially restored at N^{2}LO. At the soft cutoff $R_{NN} = 1.2$ fm in Fig. 3, this difference is smaller as the soft cutoff excludes a good deal of the chiral potentials. Going to the harder cutoff of $R_{NN} = 1.0$ fm in Fig. 4, a greater difference between the two formulations becomes evident.

The convergence pattern of the couplings is also much more systematic when Δ isobars are included explicitly. For the Δ-less case, the LO to NLO difference is quite small and the NLO to N^{2}LO difference is rather large. This pattern reflects the weakness of the NLO potential in the Δ-less theory as only the lowest order π-N vertices contribute [27]. In contrast, the couplings with Δs show a difference between LO and NLO which is larger than the difference between NLO and N^{2}LO. The improved convergence reflects the shift of more physics to the NLO potential when Δs are included and the more natural c_i coefficients.

In the $3N$ sector, we look at the couplings $g^{\rho_0^3}$ and $g^{\rho_0\rho_1^2}$. In Fig. 5, we plot these couplings as a function of the isoscalar

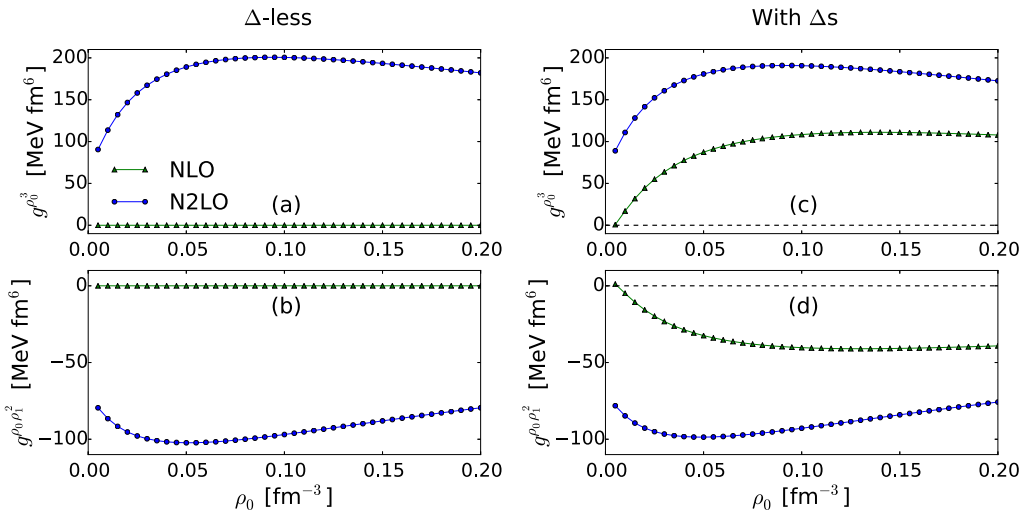

FIG. 6. The $g^{\rho_0^3}$ and $g^{\rho_0\rho_1^2}$ couplings are plotted as a function of the isoscalar density ρ_0 at fixed cutoff $R_{3N} = 1.0$ fm using the regulator in Eq. (40) with $n = 6$. The values for the couplings are shown at two different chiral orders up to N^{2}LO. The coupling $g^{\rho_0^3}$ is shown without (a) and with (c) Δ isobars. The coupling $g^{\rho_0\rho_1^2}$ is shown without (b) and with (d) Δ isobars.

density both with and without explicit Δs at a soft cutoff of $R_{3N} = 1.2\,\text{fm}$ using the regulator in Eq. (40). In Fig. 6, we plot the same couplings only now with a harder cutoff of $R_{3N} = 1.0\,\text{fm}$. Note that the couplings at NLO in the Δ-less theory are exactly zero as the $3N$ diagrams at this order vanish. Comparing the couplings at the two different given cutoffs, we do not see especially large variations, i.e., at most a factor of 2 for the N^{2}LO couplings. Furthermore at N^{2}LO, the difference in the couplings between the theory with and without Δs is small.

Although explicit Δ resonances do not show drastically different coupling behavior in the few examples here, the larger role of the Δ remains an open question. Furthermore, going to N^{3}LO in the chiral expansion, the ease with which the Δ can be implemented in our formalism will be particularly relevant. At N^{3}LO, the $3N$ force in the Δ-less theory is weak, for the same reason the NN potential is weak at NLO (only leading order π-N vertices contribute). Due to resonance saturation of the c_i coefficients, $3N$ diagrams in the Δ-less theory at N^{4}LO are therefore expected to be sizable while in the theory with Δs, these diagrams are promoted to N^{3}LO [69]. Converging the $3N$ potential may therefore be simpler when working up to N^{3}LO and including the Δ explicitly.

VIII. CONCLUSIONS

In this work, we derived density-dependent couplings from coordinate space chiral potentials working up to N^{2}LO in the chiral expansion using the DME parametrization outlined in Sec. IV C. The chiral potentials we used are derived using Weinberg power counting and come in a two versions depending on whether Δ isobars are included as explicit degrees of freedom. Our couplings are derived by applying the DME to OBDMs at the Hartree-Fock level in MBPT. Working to Hartree-Fock in MBPT is justified here due to both the softness of regulated chiral potentials and the global refit of Skyrme contacts, which are expected to mimic higher order many-body contributions. In Eqs. (47) and (48), we show the resulting EDF forms in the NN and $3N$ sector respectively. We also implemented a new organization scheme which renders tractable and modular the DME algebra associated with three-body interactions. The resulting density-dependent NN and $3N$ DME couplings then serve as input into a Skyrme-like functional. These couplings and their respective local densities can be added to a standard Skyrme functional and used in existing EDF solvers.

Our work builds upon but ultimately contrasts with the previous DME implementation in Refs. [21,22], which used chiral forces defined in momentum space and did not include ultraviolet regulators. We instead work in coordinate space and include regulators for several reasons:

(1) The DME is naturally formulated as an expansion in coordinate space about the OBDM nonlocality, with no Fourier integrals to be done for the DME coupling equations.
(2) Including an ultraviolet regulator allows for adiabatically turning on the long-range chiral potentials by changing the regularization cutoff.
(3) Coordinate space regulators, which have been shown in certain instances to better control regulator artifacts, can easily be implemented on coordinate space interactions.

Working with coordinate space interactions, numerically performing relevant integrals, and using a new robust organization scheme have also rendered the $3N$ DME implementation more transparent than the previous formulation. We hope that including regulators will address concerns with functional stability and optimization and ultimately lead to significant improvement over existing functionals, or else serve as diagnostics if improvement is not found.

Going forward, we plan to apply these DME-derived couplings in semiphenomenological calculations of nuclei and address many pertinent questions [80]: How will our new functional calculations compare with existing models? Does the refit of the Skyrme parameters adequately capture the contributions of the omitted V_D term and higher-order MBPT? Can we see evidence of pion exchange in medium and heavy nuclei? To what extent are Δ isobars important as a degree of freedom? What are the effects of including $3N$ forces in heavy systems? Can we decrease uncertainty in functional calculations to such a degree that outputs will be relevant for astrophysical and standard model experiments? Can isovector contributions in the functional be sufficiently constrained so as to make predictions in advance of the Facility for Rare Isotope Beams (FRIB)? These questions also inform how one might improve upon the present Weinberg power counting for vacuum nucleon interactions. If the addition of pion and Δ physics does not provide measurable improvement for functional calculations, these degrees of freedom may not relevant at finite density and a different EFT construction should be done for in-medium systems. This perspective would translate Skyrme functionals from a successful phenomenology to the lowest rung of a systematic EFT.

In the future, we aim to eventually construct a truly *ab initio* functional for nuclei. For such a project, reaching convergence is crucial, both in the chiral expansion and the many-body sector. The ease with which our formalism deals with including the Δ isobar then becomes particularly relevant especially with respect to $3N$ forces at N^{3}LO. For renormalization group softened chiral interactions, Hartree-Fock in MBPT becomes a quantitative starting point. However, nontrivial challenges remain both in the implementation of nonlocal softened chiral forces as well as including second-order many-body contributions. We plan to address these challenges in a future work, with the present semiphenomenological formulation being a modest step towards first-principle predictions for the full table of nuclides.

ACKNOWLEDGMENTS

We would like to thank A. Lovato, R. Navarro Perez, N. Schunck, I. Tews, and S. Wesolowski for useful discussions. We would like to especially thank T. Coello Pérez and L. Zurek for numerical comparisons and spotting two mistakes in our derivations. We are also indebted to the detailed and

precise work done by B. Gebremariam on the density matrix expansion using chiral interactions. This work was supported in part by the National Science Foundation under Grants No. PHY-1306250, No. PHY-1404159, and PHY-1614460 and the NUCLEI SciDAC Collaboration under DOE Grants No. DE-SC0008533 and No. DE-SC0008511.

[1] M. Bender, P.-H. Heenen, and P.-G. Reinhard, Rev. Mod. Phys. **75**, 121 (2003).
[2] S. Goriely, S. Hilaire, M. Girod, and S. Péru, Eur. Phys. J. A **52**, 202 (2016).
[3] T. Skyrme, Nucl. Phys. **9**, 615 (1958).
[4] D. Vautherin and D. M. Brink, Phys. Rev. C **5**, 626 (1972).
[5] J. Dobaczewski, H. Flocard, and J. Treiner, Nucl. Phys. A **422**, 103 (1984).
[6] J. Dobaczewski, W. Nazarewicz, and P. G. Reinhard, Nucl. Phys. A **693**, 361 (2001).
[7] J. Dobaczewski and W. Nazarewicz, *Fifty Years of Nuclear BCS: Pairing in Finite Systems*, edited by R. Broglia and V. Zelevinsky (World Scientific, Singapore, 2013), pp. 40–60.
[8] S. Bogner, A. Bulgac, J. A. Carlson, J. Engel, G. Fann *et al.*, Comp. Phys. Comm. **184**, 2235 (2013).
[9] K. Bennaceur and J. Dobaczewski, Comp. Phys. Comm. **168**, 96 (2005).
[10] M. Stoitsov, J. Dobaczewski, W. Nazarewicz, and P. Ring, Comp. Phys. Comm. **167**, 43 (2005).
[11] M. Stoitsov, N. Schunck, M. Kortelainen, N. Michel, H. Nam, E. Olsen, J. Sarich, and S. Wild, Comp. Phys. Comm. **184**, 1592 (2013).
[12] J. Dobaczewski and J. Dudek, Comp. Phys. Comm. **102**, 166 (1997).
[13] N. Schunck, J. Dobaczewski, J. McDonnell, W. Satuła, J. Sheikh, A. Staszczak, M. Stoitsov, and P. Toivanen, Comp. Phys. Comm. **183**, 166 (2012).
[14] N. Schunck, J. D. McDonnell, D. Higdon, J. Sarich, and S. M. Wild, Eur. Phys. J. A **51**, 1 (2015).
[15] J. D. McDonnell, N. Schunck, D. Higdon, J. Sarich, S. M. Wild, and W. Nazarewicz, Phys. Rev. Lett. **114**, 122501 (2015).
[16] N. Schunck, J. D. McDonnell, J. Sarich, S. M. Wild, and D. Higdon, J. Phys. G **42**, 034024 (2015).
[17] T. Haverinen and M. Kortelainen, J. Phys. G **44**, 044008 (2017).
[18] M. Mumpower, R. Surman, D. L. Fang, M. Beard, and A. Aprahamian, J. Phys. G **42**, 034027 (2015).
[19] M. Mumpower, R. Surman, G. McLaughlin, and A. Aprahamian, Prog. Part. Nucl. Phys. **86**, 86 (2016).
[20] B. Gebremariam, T. Duguet, and S. K. Bogner, Phys. Rev. C **82**, 014305 (2010).
[21] B. Gebremariam, S. Bogner, and T. Duguet, Nucl. Phys. A **851**, 17 (2011).
[22] M. Stoitsov, M. Kortelainen, S. K. Bogner, T. Duguet, R. J. Furnstahl, B. Gebremariam, and N. Schunck, Phys. Rev. C **82**, 054307 (2010).
[23] S. K. Bogner, R. J. Furnstahl, H. Hergert, M. Kortelainen, P. Maris, M. Stoitsov, and J. P. Vary, Phys. Rev. C **84**, 044306 (2011).
[24] S. Weinberg, Phys. Lett. B **251**, 288 (1990).
[25] S. Weinberg, Nucl. Phys. B **363**, 3 (1991).
[26] E. Epelbaum, H.-W. Hammer, and U.-G. Meißner, Rev. Mod. Phys. **81**, 1773 (2009).
[27] R. Machleidt and D. Entem, Phys. Rep. **503**, 1 (2011).
[28] R. Machleidt and F. Sammarruca, Phys. Scr. **91**, 083007 (2016).
[29] E. Jenkins and A. V. Manohar, Phys. Lett. B **259**, 353 (1991).
[30] T. R. Hemmert, B. R. Holstein, and J. Kambor, Phys. Lett. B **395**, 89 (1997).
[31] J. Carlson, S. Gandolfi, F. Pederiva, S. C. Pieper, R. Schiavilla, K. E. Schmidt, and R. B. Wiringa, Rev. Mod. Phys. **87**, 1067 (2015).
[32] R. Roth, J. Langhammer, A. Calci, S. Binder, and P. Navratil, Phys. Rev. Lett. **107**, 072501 (2011).
[33] T. A. Lähde, E. Epelbaum, H. Krebs, D. Lee, U.-G. Meißner, and G. Rupak, Phys. Lett. B **732**, 110 (2014).
[34] K. Tsukiyama, S. K. Bogner, and A. Schwenk, Phys. Rev. C **85**, 061304 (2012).
[35] G. R. Jansen, J. Engel, G. Hagen, P. Navratil, and A. Signoracci, Phys. Rev. Lett. **113**, 142502 (2014).
[36] S. R. Stroberg, H. Hergert, J. D. Holt, S. K. Bogner, and A. Schwenk, Phys. Rev. C **93**, 051301 (2016).
[37] V. Soma, T. Duguet, and C. Barbieri, Phys. Rev. C **84**, 064317 (2011).
[38] V. Somà, A. Cipollone, C. Barbieri, P. Navrátil, and T. Duguet, Phys. Rev. C **89**, 061301 (2014).
[39] H. Hergert, S. Binder, A. Calci, J. Langhammer, and R. Roth, Phys. Rev. Lett. **110**, 242501 (2013).
[40] H. Hergert, S. K. Bogner, T. D. Morris, S. Binder, A. Calci, J. Langhammer, and R. Roth, Phys. Rev. C **90**, 041302 (2014).
[41] S. Gandolfi, A. Lovato, J. Carlson, and K. E. Schmidt, Phys. Rev. C **90**, 061306 (2014).
[42] D. Lee, Prog. Part. Nucl. Phys. **63**, 117 (2009).
[43] G. Hagen, T. Papenbrock, M. Hjorth-Jensen, and D. J. Dean, Rept. Prog. Phys. **77**, 096302 (2014).
[44] H. Hergert, S. Bogner, T. Morris, A. Schwenk, and K. Tsukiyama, Phys. Rep. **621**, 165 (2016).
[45] B. R. Barrett, P. Navratil, and J. P. Vary, Prog. Part. Nucl. Phys. **69**, 131 (2013).
[46] S. K. Bogner, R. J. Furnstahl, and A. Schwenk, Prog. Part. Nucl. Phys. **65**, 94 (2010).
[47] K. Hebeler, S. K. Bogner, R. J. Furnstahl, A. Nogga, and A. Schwenk, Phys. Rev. C **83**, 031301 (2011).
[48] S. K. Bogner, R. J. Furnstahl, and L. Platter, Eur. Phys. J. A **39**, 219 (2009).
[49] J. E. Drut, R. J. Furnstahl, and L. Platter, Prog. Part. Nucl. Phys. **64**, 120 (2010).
[50] J. W. Negele and D. Vautherin, Phys. Rev. C **5**, 1472 (1972).
[51] J. W. Negele and D. Vautherin, Phys. Rev. C **11**, 1031 (1975).
[52] B. Gebremariam, S. Bogner, and T. Duguet, Comp. Phys. Comm. **181**, 1167 (2010).
[53] J. W. Holt, N. Kaiser, and W. Weise, Prog. Part. Nucl. Phys. **73**, 35 (2013).
[54] A. Gezerlis, I. Tews, E. Epelbaum, S. Gandolfi, K. Hebeler, A. Nogga, and A. Schwenk, Phys. Rev. Lett. **111**, 032501 (2013).
[55] A. Gezerlis, I. Tews, E. Epelbaum, M. Freunek, S. Gandolfi *et al.*, Phys. Rev. C **90**, 054323 (2014).

[56] J. E. Lynn, J. Carlson, E. Epelbaum, S. Gandolfi, A. Gezerlis, and A. Schwenk, Phys. Rev. Lett. **113**, 192501 (2014).
[57] J. E. Lynn, I. Tews, J. Carlson, S. Gandolfi, A. Gezerlis, K. E. Schmidt, and A. Schwenk, Phys. Rev. Lett. **116**, 062501 (2016).
[58] I. Tews, S. Gandolfi, A. Gezerlis, and A. Schwenk, Phys. Rev. C **93**, 024305 (2016).
[59] A. Dyhdalo, R. J. Furnstahl, K. Hebeler, and I. Tews, Phys. Rev. C **94**, 034001 (2016).
[60] E. Epelbaum, H. Krebs, and U. G. Meißner, Eur. Phys. J. A **51**, 53 (2015).
[61] See Supplemental Material at http://link.aps.org/supplemental/10.1103/PhysRevC.95.054314 for full two- and three-body potentials, three-body DME expansion example, single and double exchange three-body traces, single and double exchange three-body DME dictionaries, and full expressions for three-body DME couplings.
[62] D. Sprung, M. Vallieres, X. Campi, and C.-M. Ko, Nucl. Phys. A **253**, 1 (1975).
[63] B. Gebremariam, Ph.D. thesis, Michigan State University, East Lansing, 2010 (unpublished).
[64] A. Ekström, G. Baardsen, C. Forssén, G. Hagen, M. Hjorth-Jensen, G. R. Jansen, R. Machleidt, W. Nazarewicz, T. Papenbrock, J. Sarich, and S. M. Wild, Phys. Rev. Lett. **110**, 192502 (2013).
[65] A. Ekström, G. R. Jansen, K. A. Wendt, G. Hagen, T. Papenbrock, B. D. Carlsson, C. Forssén, M. Hjorth-Jensen, P. Navrátil, and W. Nazarewicz, Phys. Rev. C **91**, 051301 (2015).
[66] M. Piarulli, L. Girlanda, R. Schiavilla, R. N. Pérez, J. E. Amaro, and E. R. Arriola, Phys. Rev. C **91**, 024003 (2015).
[67] E. Epelbaum, H. Krebs, and U.-G. Meißner, Nucl. Phys. A **806**, 65 (2008).
[68] V. Bernard, N. Kaiser, and U.-G. Meißner, Nucl. Phys. A **615**, 483 (1997).
[69] R. Machleidt and D. R. Entem, J. Phys. G **37**, 064041 (2010).
[70] I. Tews, Ph.D. thesis, Technische Universität Darmstadt, Darmstadt, Germany, 2015 (unpublished).
[71] J.-i. Fujita and H. Miyazawa, Prog. Theor. Phys. **17**, 360 (1957).
[72] U. van Kolck, Phys. Rev. C **49**, 2932 (1994).
[73] E. Epelbaum, A. Nogga, W. Glockle, H. Kamada, U.-G. Meißner, and H. Witala, Phys. Rev. C **66**, 064001 (2002).
[74] A. Lovato, O. Benhar, S. Fantoni, and K. E. Schmidt, Phys. Rev. C **85**, 024003 (2012).
[75] E. Perlińska, S. G. Rohoziński, J. Dobaczewski, and W. Nazarewicz, Phys. Rev. C **69**, 014316 (2004).
[76] S. G. Rohoziński, J. Dobaczewski, and W. Nazarewicz, Phys. Rev. C **81**, 014313 (2010).
[77] X. Campi and A. Bouyssy, Phys. Lett. B **73**, 263 (1978).
[78] H. Krebs, E. Epelbaum, and U.-G. Meißner, Eur. Phys. J. A **32**, 127 (2007).
[79] D. Siemens, V. Bernard, E. Epelbaum, A. Gasparyan, H. Krebs, and U.-G. Meißner, Phys. Rev. C **94**, 014620 (2016).
[80] R. N. Pérez, A. Dyhdalo, N. Schunck, S. Bogner, and R. J. Furnstahl (unpublished).